THE PENNSYLVANIA STATE UNIVERSITY
SCHREYER HONORS COLLEGE

DEPARTMENT OF CHEMISTRY

SYNTHESIS AND ANALYSIS OF ATP-INDEPENDENT ENZYME-POWERED MICROPUMPS

ARJUN AGRAWAL
SPRING 2015

A thesis
submitted in partial fulfillment
of the requirements
for a baccalaureate degree
in Biology
with honors in Chemistry

Reviewed and approved* by the following:

Ayusman Sen
Distinguished Professor of Chemistry
Thesis Supervisor

Raymond Funk
Professor of Chemistry
Honors Advisor

* Signatures are on file in the Schreyer Honors College.

ABSTRACT

The next generation of smart devices will need to incorporate the ability to self-regulate, in the absence of a constantly supplied source of energy, and be bio-friendly. The system demonstrated here displays these characteristics using enzymatic reactions as a power source for micropumps that can be used for sensing and detection.

Surface-immobilized enzymes can function as both sensors and micropumps that create the pumping of fluid in a directional manner in response to increasing substrate concentration. These systems are independent of cellular energy in the form of adenosine triphosphate, and depend only on the enzyme's substrate to create fluid flow. They are minutely self-regulating depending on the amount of substrate concentration available in surrounding fluid. The robustness of this system was demonstrated via spatial and temporal analysis, and the pumping mechanism was determined to be density-dependent.

These surface-immobilized enzyme systems were then adapted for use in more biocompatible hydrogel scaffold systems. These gels could be loaded with small molecules such as dyes or drugs and pump these molecules out in the presence of substrate. It was demonstrated here that enzymes electrostatically attached to the surface of gels could be used to generate fluid flows through their pumping mechanism and help to actively release various concentrations of drug in response to substrate concentration. This led to the eventual design of two important systems, one which pumped out insulin in the presence of glucose, and another which rapidly pumped out 2-PAM, a potent antidote to treat nerve agent poisoning. The creation of these systems will be intrinsic to the next generation of smart devices as sensors and pumps, potentially for use within the human body.

TABLE OF CONTENTS

LIST OF FIGURES

LIST OF TABLES

ACKNOWLEDGEMENTS

I would like to begin by thanking Dr. Sen for giving me the tremendous opportunity of working in his lab these past three years. It has truly been the most rewarding experience of my college career. I still remember the day that I nervously interviewed with him after taking his general chemistry class, and his skepticism at having a biology student work in his chemistry lab. I can only hope that I have exceeded his expectations.

I would like to thank Dr. Samudra Sengupta, my first mentor in this lab, for putting up with me when I was just a freshman who had never even used a real microscope before. Answering my incessant questions (often the same one), being the reassuring hand watching over my work, and quickly forgiving me when I made mistakes are things that I valued more than he knew. I met him that very first day that I interviewed with Dr. Sen, and his passion for his work and enthusiasm about working in the lab is what drew me to him and this lab. He taught me how to be a researcher, gave me confidence, and pushed me enough to be successful.

I would like to thank my current mentor, future Dr. Isamar Ortiz-Rivera, for her unwavering support and putting up with my banter and occasional antics. I always appreciate her several-minute-long explanations to each of my questions, her intense sense of organization, and her willingness to go above and beyond your duties to help. She introduced me to her wonderful world of gels, and despite the troubles that we had, she showed me some of the most fun experiments that I engaged in. She also take great care to consider what all I had going on before planning experiments and made sure I wasn't overwhelmed at the lab. I know I may not show it through the teasing and fun we had together, but I am truly thankful to have had her as a mentor.

To my friends and current/former coworkers in lab, Deb, Lyanne, Krishna, Frances, Flory, Chandrani, and Scott, I would like to thank them for making this lab an enjoyable and interesting place to work. Their enthusiasm for being in lab, their overall demeanor, and the fun we had together was something that made the lab not somewhere I had to be, but somewhere I wanted to be. I want to thank them for making that a possibility. A special thanks also to Isamar, Lyanne and Krishna for the editing of this thesis. This literally would not have been possible without them.

To my friends outside the lab, Jullien, Geoffrey, Michael, Div, Nick, Allen, Luke, Alyssa, Nick, and Nic, and to any of whom not mentioned, I would like to thank for being there to keep me sane outside of lab, for enduring my sometimes erratic schedule, and for keeping the rest of college life fun and interesting.

Last, but certainly not least, I would like to thank my parents, Atul and Kumud Agrawal, for their unwavering support through my entire life, including my college career and this thesis. For being there when experiments didn't work, for staying on speakerphone some late nights in the lab, and for telling me when it was time to back down and take some time off, I am truly grateful. I still remember their enthusiasm at my first publication, and making them proud is what keeps me going. Without their support, this thesis aside, none of what I have accomplished would ever have been possible.

Chapter 1 : Background

1.1 Introduction

Almost every technological invention that mankind has made has been progressively becoming smaller. From gasoline engines to USB memory, inventions have become more compact, yet more powerful. One key area of miniaturization is the relatively new area of nano-medicine, where site-specific drug delivery is a field of great interest. Current generations of devices that are involved in nanoscale medicine rely on the circulatory system, and specific carriers such as liposomes[1], emulsions[2], and micelles[3] passively move towards their targets. A new generation of smart nano-medical devices could be drug delivery systems that autonomously deliver, via manipulation of local fluid flows, their molecules of interest to the desired target via their response to paracrine or endocrine biomolecules.

The most useful microscale bio-devices will be those that are able to sense and respond to environmental stimuli. Chemical reactions can be used to change material properties in a way that allows for the production of mechanical force, triggering a response.[4] This method of chemically-induced sense and response allows for a microscale device that does not require any wires to function autonomously, an important requirement for potentially bio-compatible devices.[5] Furthermore, this chemical activation of an autonomous mechanical response eliminates the necessity for an external power source, allowing for countless applications.

The next generation of smart devices will need to incorporate microscale capabilities, require little to no energy source, and be able to be precisely regulated. Enzymes, which are biological catalysts, are the perfect candidates to generate devices such as this, and may prove to be essential to creating minutely-regulated energy-independent non-mechanical devices.

Enzymes may act as both sensors and pumps, allowing for a unique advantage in bottom-up assembly of specific structures, or mediated cargo-delivery, such as drug delivery. In addition, enzymes are biocompatible and hence devices containing enzymes as catalytic motors are less likely to be rejected by the host's immune system.

Single enzyme molecules have been shown to be diffusively motile when exposed to a gradient of substrate in a substrate concentration dependent manner, and even exhibit chemotaxis when aggregates of enzymes are exposed to these gradients.[6-8] When fixed in place, these enzymes which move through a fluid via a continuous surface force should instead be able to pump fluid in a directed manner.

This research aims to discuss the methods, results, and applicability of creating such microscale ATP-independent regulated fluid-dynamic pumps using a variety of enzyme-substrate systems. A prototype chemomechanical device that combines sensing and microfluidic pumping was created and it was analyzed in a substrate-concentration-dependent manner using UV/optical microscopy and other analytical techniques. Furthermore, an enzyme-immobilized hydrogel was created as a proof-of-concept device as a bioengineered construct for the release of a drug molecule in response to appropriate chemical stimuli.

1.2 Enzymes: Biological Catalysts

Enzymes are biological catalysts, which are distinct from other chemical catalysts in several ways. Enzymes act similarly to other chemical catalysts in that they speed up reaction rates, however enzymes also allow for milder reaction conditions, greater reaction specificity,

and a capacity for regulation.[9] These properties make enzymes ideal systems for use in microscale smart devices.

Enzymes come in many shapes and sizes, and catalyze a variety of different reactions. They are categorized based on the type of chemical reaction they catalyze. For instance, oxidoreductase enzymes catalyze oxidation-reduction reactions. Transferases catalyze the transfer of functional groups from one macromolecule to another. Hydrolases catalyze hydrolysis reactions, while lyases catalyze reactions that form double bonds.[9]

Greater reaction specificity is achieved when using enzymes as they only attach to certain substrates, which are determined by the enzyme's active site. The active site is the catalytic portion of the enzyme molecule, where the actual chemical reaction takes place. This catalytic site contains a substrate binding pocket which is geometrically complementary to the enzyme's substrate. The side chains that form the active site are also electronically complementary to the substrate, and aid to attract the substrate and place it properly in the substrate-binding pocket. Most enzymes undergo a slight conformational change upon binding of the substrate in order to become more efficient catalysts.[9]

Enzymes generally act to speed up chemical reactions by reducing the energy of activation. The activation energy step is typically the rate-limiting step in chemical reactions, and the enzymes are able to stabilize the transition state of the interacting molecules. This stabilization reduces the energy of activation, thereby speeding up the reaction process. This stabilization occurs in both directions of the reaction coordinate, allowing for equilibrium to be reached at a greater rate.[9]

1.3 Enzyme Kinetics

All enzymes can be analyzed to determine their reaction rates and overall efficiency. Enzyme interactions involve the enzyme, the substrate, the enzyme-substrate complex, and the product. Enzyme kinetics are typified primarily by the Michaelis-Menten equation, which assumes that the enzyme-substrate complex remains in a steady state.[9]

The steady-state assumption is critical to the applicability of the Michaelis-Menten equation. There are two basic components to this: the assumption of equilibrium and the assumption of steady state. The assumption of equilibrium states that the first step of the reaction, that of the enzyme and substrate forming the enzyme-substrate complex, exist in equilibrium. The enzyme-substrate complex is also known as the Michaelis complex. The steady state assumption postulates that the amount of the enzyme-substrate complex remains constant until there is little to no substrate left in solution. This allows for the concentration of the enzyme-substrate complex to be treated as a constant.[9]

The concentration of enzyme (E) and enzyme-substrate complex (ES) are not directly measurable. However, the total enzyme concentration is measurable, as the sum of E and ES. The Michaelis Constant, K_M is then defined as the rate of the conversion from ES to E + S (k_{-1}) plus the rate of formation of product (k_2) divided by the rate of formation of ES (k_1).[9] This relationship is described in the following equation:

$$K_M = \frac{k_{-1} + k_2}{k_1}$$

Equation (1): The Michaelis Constant

In order to meet the requirements of the steady state assumption, the substrate concentration must greatly exceed the enzyme concentration. Thus, the maximal rate of reaction,

V_{max} occurs when the enzyme is saturated with its substrate. We can then solve for the initial rate of reaction, v_o using V_{max}, K_M, and the substrate concentration. This gives us the true Michaelis-Menten equation.[9] The equation is shown below:

$$v_o = \frac{V_{max}[S]}{K_M + [S]}$$

Equation (2): The Michaelis-Menten Equation

The Michaelis-Menten equation allows us to determine that K_M when equal to the substrate concentration, allows the velocity of the reaction to be half $V_{max.}$ This relationship essentially means that the smaller the K_M of an enzyme, the less substrate it requires to reach catalytic efficiency. K_M values differ for each enzyme-substrate complex, and hence the same enzyme can have different catalytic efficiency given different substrates or even different variants of the same substrate.[9]

A separate constant, the catalytic constant (k_{cat}) can also be determined. This constant is also known as the turnover number of the enzyme. It represents the number of reactions that each enzyme can catalyze per a unit time. The overall rate of the reaction being catalyzed varies with the rate at which the enzyme and substrate interact with each other. This can be expressed via the relation k_{cat}/K_M, which is considered a measure of the enzyme's catalytic efficiency. However, the k_{cat}/K_M cannot exceed the value of k_1, as product cannot be made at a rate greater than that of the interaction of the reactants.[9]

1.4 The Physics of Motion at the Nanoscale

When considering systems at the nanoscale, the specific physics of the system must be taken into account. Objects on the microscale do not move in a manner exactly similar to that on the macroscale. The physics of motion at the nanoscale is actually quite different from the macroscopic world we all experience. The manipulation of motion at the nanoscale has been an area of research for quite some time, as there are a number of differences that have to be taken into account. Though there are many different aspects of the physical world at the nanoscale, we will take into account only those which are most relevant to enzyme-micropump systems, namely the Reynolds number and Brownian motion/diffusion.

The Reynolds number (Re) is a dimensionless quantity that relates the density of the fluid, the velocity of particles, the length of the system, and the viscosity of the fluid. It is given by the relation shown below in Equation 3.

$$\mathrm{Re} = \frac{\mu V^2 L^2}{\mu V L}$$

Equation (3): The Reynolds Number

In this equation, the density of the fluid is given by (ρ), the velocity of the object being studied (V), the length of the system (L), and the viscosity of the fluid (μ).[10] The Reynolds number effectively demonstrates the ratio of inertial forces to viscous forces. In our macroscale world, generally inertial forces are predominant. This is considered a high Reynolds number system. However, on the microscale and smaller, viscous drag forces become predominant. In this case, inertial forces become basically nonexistent, and the Reynolds number becomes very low. In this low Reynolds number scenario, any force exerted on an object is countered immediately by a viscous drag force.[11] Effectively, this means that only the instantaneous forces

upon an object determine that object's motion. Past forces do not contribute to any inertial motion. This means that in order for objects to move in a fluid system on the microscale/nanoscale, there must be a constant force exerted upon them.

A somewhat related concept to the Reynolds number, specifically low Reynolds number motion, is Brownian motion. This is a random process, which is due to continuous collisions of solvent molecules with the object in question's surface, thereby transferring some amount of momentum to the object. In macrosystems, with high Reynolds number, the amount of momentum carried by solvent molecules is largely negligible, due to the scale of the object. However, in microsystems, these effects cannot be ignored and can have significant impact on the motion of small objects.[12] In addition, the reduced surface area of microparticles reduces the probability that collisions with solvent molecules will occur at opposite ends and cancel each other out.

Brownian diffusion is approximated by the diffusion constant (D) and depends on the absolute temperature of the solution (T), the viscosity of the fluid (η) and the hydrodynamic radius (R_H) of the object.[13] The equation is shown below:

$$D = \frac{k_B T}{6\pi\eta R_H}$$

Equation (4): Brownian Diffusion Coefficient

Based on the equation above, it follows that the denominator represents the viscous drag coefficient. As the size of the molecules decreases, the randomness of their motion increases.[13]

1.5 Nanoscale Kinetic Mechanisms

When characterizing these enzyme micropumps, special attention must be paid to the specific mechanism of their pumping action. As the physics of motion at the nanoscale differs from that at the macroscale, there are a number of kinetic mechanisms that the enzyme pumps may employ in order to achieve directional fluid flow. Some of the most important mechanisms for our purposes are self-electrophoresis, electrolytic and non-electrolytic diffusiophoresis, and bubble propulsion. These will be discussed in further detail.

1.5.1 Self-Electrophoretic Motion

Electrophoresis occurs when a charged object moves across an electric field. When an electric field is generated across a motor in a fluid, the field causes the charges on the surface of the motor to move, creating a slip velocity. Thus, the fluid can flow freely around the object, causing the motor to be forced in the opposite direction as the field.[13] The velocity of this motion can be calculated via the following equation:

$$U = \frac{\varepsilon \zeta E}{\eta}$$

Equation (5): Self-Electrophoretic Velocity

In Equation 5, U represents the velocity, the dielectric constant of the solution is represented by ε, the zeta potential of the object is represented by ζ, and E represents the magnitude of the electric field, while η represents the viscosity.[13]

1.5.2 Electrolytic Diffusiophoretic Motion

When a gradient of electrolytes is created close to a charged surface, electrolytic diffusiophoresis can occur. This incorporates both an electrophoretic effect and a chemiphoretic effect. The interaction between a charged surface and a fluid causes a double layer to be formed, whereby two parallel opposing layers of charge form at the interface. One layer is of the material itself, where the intrinsic properties of the material create a surface charge. The second layer occurs due to the electrostatic effect, where ions in solution migrate toward the surface charge.[14] The equation for this velocity is given below:

$$U = \left[\frac{d\ln(C)}{dx}\right]\left[\frac{D_C - D_A}{D_C + D_A}\right]\left[\frac{k_B T}{e}\right]\left[\frac{e\left(\zeta_p - \zeta_w\right)}{\eta}\right] + \left[\frac{d\ln(C)}{dx}\right]\left[\frac{2\varepsilon k_B^2 T^2}{\eta e^2}\right]\left\{\ln\left[1-\tanh^2\left(\frac{e\zeta_w}{4k_B T}\right)\right] - \ln\left[1-\tanh^2\left(\frac{e\zeta_p}{4k_B T}\right)\right]\right\}$$

Equation (6): Velocity due to Electrolytic Diffusiophoresis

In the above equation, the velocity of the particles near a wall is given by U, where k_B is the Boltzmann constant, temperature is T, e is the charge of the electron, $d\ln(C)/dx$ is the electrolyte gradient, D_C is the diffusion coefficient of the cation, D_A being the diffusion coefficient of the anion, ξ_p being the zeta potential of particles, and ζ_W the zeta potential of the wall.[15] The electrophoretic effect is contained in the first term, while the chemophoretic effect is represented by the second part of the equation. The electrophoretic effect occurs as a result of a difference in diffusion rates between the cation and anion electrolytes involved in the gradient. As the ion spreads through a solution, the separation of charges will generate local electrical fields to counteract the difference in diffusion rates of the ions involved. These electric fields will not only exert an effect on the ions diffusivity, but also affect the movement of other charged surfaces in solution.

Simultaneously, the ion gradient will form a concentration gradient, which will generate a pressure difference in the double layer present on charged surfaces. This causes the solvent molecules in the double layer to flow from areas of high solute concentration to areas of low solute concentration, resulting in what is known as chemiphoretic flow. Both the electrophoretic movement and chemiphoretic movement combined result in diffusiophoretic motion.[15]

1.5.3 Non-electrolytic Diffusiophoretic Motion

This type of motion is due to the gradient of uncharged solute molecules across a surface. Solute molecules interact with the surface of the object of interest and affect the velocity of the object in a positive or negative manner, depending on whether the solute-object interaction is repulsive or attractive. The equation for velocity due to non-electrolytic diffusiophoresis is given below.

$$U = \frac{k_B T}{h} KL\nabla C$$

Equation (7): Velocity due to Non-eletrolyte diffusiophoresis

In the above equation, the velocity (U) is a function of the temperature (T), the Boltzmann constant (k_B), the viscosity of the fluid (η), the Gibbs absorption length (K), the length of the solute-object interaction (L), and the concentration gradient ∇C.[13] There are a distinct set of advantages and disadvantages found for each of the two diffusiophoretic mechanisms. Due to its absence of surface charge, non-electrolytic diffusiophoretic mechanisms are capable of working in high ionic-strengh solutions. However, at low ionic strengths, electrolytic diffusiophoresis can yield greater velocities. If the two effects by which the solvent is attracted to the gradient are comparable, namely electrostatic or van der waals interactions, then

the electrolytic diffusiophoretic mechanism is stronger due to its one additional electrophoretic component.

1.5.4 Bubble Propulsion

Bubble propulsion is a method of simple directional fluid flow. Bubbles are created on the catalytic side of a given motor, and the force from the bubble's dissolution causes motion. This mechanism works over a gradient, as bubbles must be produced only on one side of the catalyst so as to achieve directional fluid flow.[16]

1.6 Conclusion

In this chapter we have discussed the various reasons by which enzyme-powered micropumps are likely to be the next generation of autonomous self-regulated microdevices. We went through the basics of enzymes as catalysts and enzyme kinetics, as well as various mechanisms of fluid flow that can be exacted by enzyme pumps. We also briefly discussed the nature of physics and movement at the microscale, and how it differs from that of the macroscale world. The next chapter will focus on a novel microfluidic enzyme-micropump device, created by means of a self-assembled monolayer of enzyme that can exact directional fluid flow. This device will be further characterized by a variety of assays, and its mechanism of pumping determined. This device may serve as a basis for many future potential applications of enzyme-powere micropumps, including hydrogel scaffolds and beyond. The possibilities for use as sensors and biocompatible devices are limitless.

Chapter 2 : Enzyme Powered Micropumps

2.1 Introduction

The next generation of smart devices will need to incorporate multi-functional capabilities, require little to no energy source, and be able to be precisely regulated. Enzymes, which are biological catalysts, are the perfect candidates to generate devices such as this, and may prove to be essential to creating minutely-regulated energy-independent non-mechanical devices. Enzymes may act as sensors and pumps, allowing for a unique advantage in bottom-up assembly of specific structures, or mediated drug-delivery devices. In addition, enzymes are biocompatible and hence devices containing enzymes as catalytic motors are less likely to be rejected by the host's immune system.

Pumps that would be most ideal and applicable to the most scenarios are those that are responsive to the concentration of a system-specific analyte, such as an enzyme's substrate. Biocompatible, external energy source independent micropumps would be ideal for a variety of situations such as drug delivery or as biological sensors. This chapter focuses on the synthesis and characterization of such a device, one that is able to self-assemble into a complex structure to achieve a simultaneous action, does not require any external power source or even require cellular energy (ATP), and is highly responsive to a specific analyte in solution. Various opportunities exist for the use of these enzyme-powered, ranging from the field of healthcare to water treatment, and the potential applications are limitless.

2.2 Experimental Methods[42]

2.2.1 Micropump Design and Enzyme Immobilization

Gold (Au) was patterned onto a PEG-coated glass slide (MicroSurfaces) using an e-beam evaporator. Au was patterned at a thickness of 90 nm on the PEG-functionalized surface, with a 10 nm adhesion layer of chromium (Cr). The Au pattern was created with a radius of 3 mm. The evaporated Au surface on the PEG-coated glass slide was then cleaned thoroughly, being washed first with isopropanol and then with acetone, and finally dried with nitrogen. A synthesized quaternary-ammonium-thiol linker was used to create a self-assembled monolayer (SAM) formation on the Au surface. The surface was incubated overnight in a solution of the quaternary ammonium thiol linker dissolved in methanol under an inert atmosphere.

After 24 hours the surface was washed several times with methanol, followed by 10 mM Phosphate Buffered Saline (PBS) buffer, and then dried under an inert atmosphere. This functionalized SAM-modified surface was incubated in a solution of desired enzyme for 4-6 hours. Enzymes, bearing a negative charge, selectively bound to the thiol-functionalized Au-patterned surface via an electrostatic assembly. To remove unbound enzyme molecules from the PEG-coated glass slide, this new enzyme-functionalized surface was then thoroughly washed with 10 mM PBS. The area surrounding the Au pattern was then quickly dried and the Au-patterned surface was covered with a secure-seal hybridization chamber (Electron Microscopy Sciences) that was 20 mm in diameter and 1.3 mm in height.

2.2.2 Raw Video Data Collection and Particle Tracking

The fluid flow was monitored using functionalized polystyrene microspheres (Polysciences Inc.) that were 2 μm in size that acted as tracers. They were suspended in a buffered solution of substrate for each experiment.

Raw data was collected as videos of each experiment were taken, captured on two different optical setups. The first was an upright optical microscope (Olympus BX60M) equipped with a halogen lamp (12 V max, 100 W). Excitation light was focused into the sample patch through a 50x objective (LMPlanFLN 50x/0.5 BD∞/0/FN26.5, Olympus) and emission light was collected by the objective and passed through interference fiters before being detected by a high sensitivity CCD camera at 30 frames per second. Raw videos were recorded using this CCD camera that was attached to the optical microscope.

The other setup also utilized the optical microscope, consisting of an inverted microscope (Zeiss Axiovert 200 MAT) with a halogen lamp (12 V max, 100 W). The excitation light was focused into the sample via a 20x objective (EC Epiplan-NEUFLUAR 50×/0.55 HD DIC ∞/0, Zeiss) or a 50x objective (LD EC Epiplan-NEOFLUAR 20×/0.5 HD DIC 422472-9960, Zeiss). The emission light was collected by the objective, before passing through interference filters and being detected by a high sensitivity FLEA 3 CCD camera (FL3-U3-32S2C-CS, Point Grey), with a resolution of 2080/1552 pixels at 30 frames per second. Raw videos were recorded using this camera, which was attached to the optical microscope. Fluid pumping velocity was then measured by tracking 30 tracer particles over a 25 second time interval using PhysVis software (Kenyon College).

2.2.3 Synthesis of Quaternary Ammonium Thiol Linker

The quaternary ammonium thiol that acts as a linker to bind the enzyme molecules to the Au-patterned surface via electrostatic interactions was synthesized using a previously reported procedure.[43] The NMR data for the final product of the reaction scheme corresponded well with the values that were reported in the literature. The reaction scheme is shown below, in Figure 2-1.

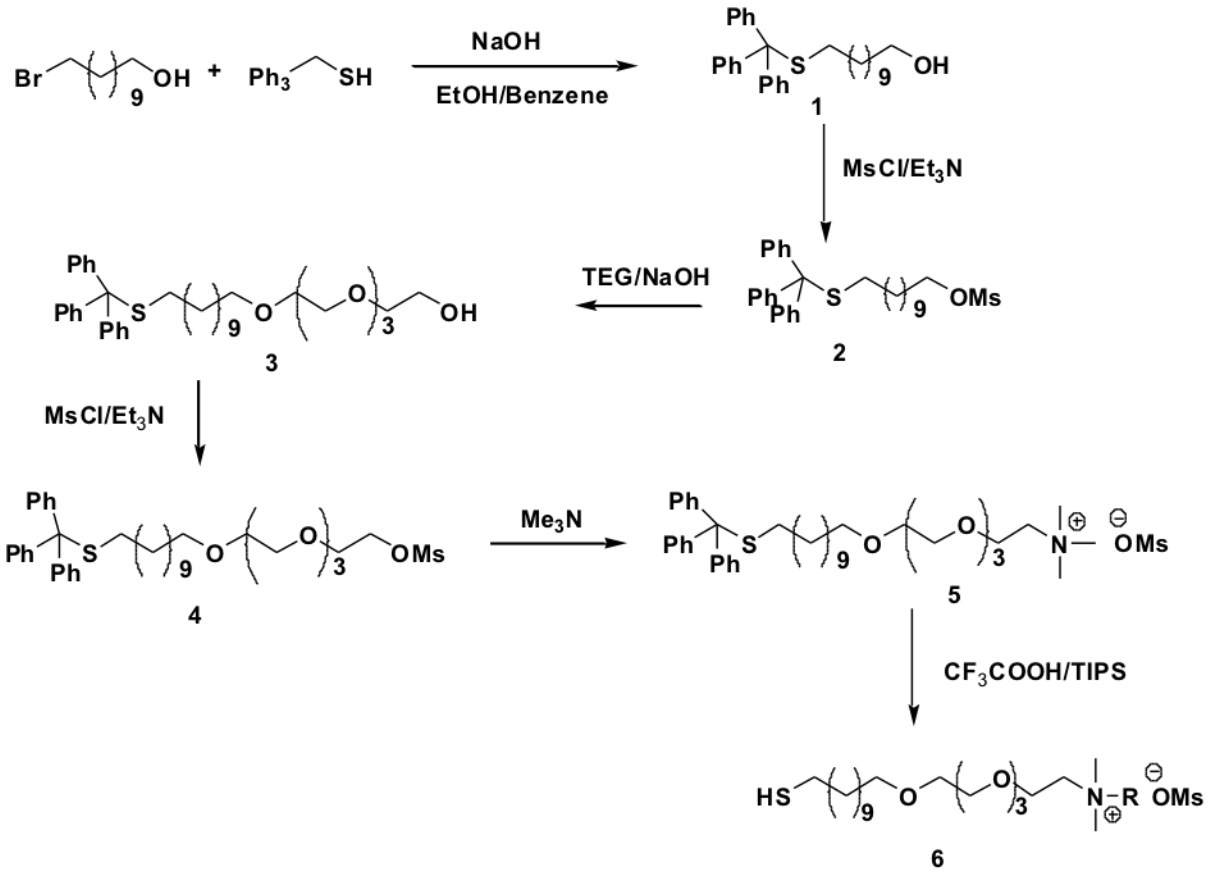

Figure 2-1: Schematic of synthesis of quaternary ammonium thiol linker

2.2.4 Fluorescent Labeling and Enzyme Immobilization

Catalase from Bovine liver (Sigma-Aldrich) was labeled using amine-reactive rhodamine dye (Ex/Em: 552/575; Thermo Fisher Scientific). Labeling of the enzyme (4 μM) was done with the fluorescent dye (40 μM) in gently stirred, room temperature 100 mM phosphate buffer (pH 7.2) for 2 hours. To eliminate unbound dye molecules from the reaction mixture, the solution was purified via membrane dialysis (10 kDa pores; Amicon ultra-4 centrifugalfilter unit, Millipore). The SAM-modified Au-patterned surface was then functionalized with the fluorescent tag enzyme molecules via an electrostatic assembly as previously detailed in Section 2.2.1.

2.2.5 Fluorescence Imaging

SAM-modified Au pattern that was functionalized with fluorescent-labeled enzyme molecules was viewed under a fluorescence-imaging microscope. Images were captured using an optical upright microscope (Olympus BX51) with a halogen lamp (100 W). Excitation light passed through the appropriate filter cube for the excitation/emission wavelengths of the dye, before the light became focused onto the sample through a 10x objective (UPlanFL 10×/0.30 ∞/-, Olympus). The fluorescent emission was collected by the objective, passed through interference filters, and detected by a high sensitivity CCD camera.

2.2.6 Calculation of Reaction Rate

The pumping velocity of enzyme-powered micropumps was measured in a substrate-concentration dependent manner, which is related to the reaction rate. The Michaelis-Menten equation relates both substrate concentration and reaction rate, and is given by the following formula:

$$v = \frac{V_{\max}[S]}{K_M + [S]}; V_{\max} = k_{cat}[E]$$

Equation (2): The Michaelis-Menten Equation

In the above equation, ν is the reaction rate, V_{max} is the maximal reaction rate, which is also equivalent to k_{cat}, the turnover number multiplied by the concentration of enzyme [E]. [S] is the substrate concentration and K_M is the Michaelis constant, the substrate concentration at which the reaction rate is equal to $V_{max}/2$. The reaction rates for each substrate concentration were determined using literature values of k_{cat} and K_M for free enzymes in solution. It should however be noted that these values will differ for enzymes immobilized on a surface, as part of the molecular structure has been restricted by the scaffold. The Au pattern was assumed to be covered by a monolayer of the quaternary ammonium thiol linker-bound enzymes in a tightly packed manner. The enzyme concentration was determined using the hydrodynamic radius of the enzyme, with the assumption that each enzyme is roughly spherical.

The amount of enzyme attached to the pattern was roughly estimated by taking into account the surface area of the pattern (28.27 mm^2) and the surface area of the various enzymes. Using the conversion factor of Avogadro's number (6.02 x 10^{23} molecules/mole), the moles of enzyme was determined (5.7 x 10^{13} moles), and the overall concentration was calculated by

incorporating the volume of solution contained by the spacer (4.084 x 10^{-7} m^3). An example of this calculation of reaction rate is given in the following section.

Example calculation of reaction rate using catalase:

The area of the gold patch can be determined via its radius. This calculation is shown below:

$$\pi \times \left(3 \times 10^{-3}\right)^2 m^2 = 2.8 \times 10^{-5} m^2$$

The diameter of a single catalase molecule was found to be 10.2 nm.[18] The cross sectional area of the molecule was therefore determined via the following calculation:

$$\frac{\pi \times \left(10.2 \times 10^{-9}\right)^2}{4} m^2 = 8.2 \times 10^{-17} m^2$$

Thus from these numbers the approximate number of enzyme molecules found on the gold pattern was determined.

$$[E] = \frac{5.7 \times 10^{-13} moles}{0.0004084\ L} = 1.40 \times 10^{-9} M$$

Catalase was assumed to have four active sites per molecule of enzyme, multiplying our Michaelis-Menten equation by a factor of four. The K_M for bovine liver catalase was found to be 93 mM, and the following rate calculation is for the maximal substrate concentration of 100 mM.

$$v = \frac{4 k_{cat} [E][S]}{K_M + [S]}$$

k_{cat} (*catalase, per active site*) = $2.12 \acute{} \ 10^5 s^{-1}$[19]

$$v = \frac{4\left(2.12 \times 10^5 s^{-1}\right)\left(1.40 \times 10^{-9} M\right)\left(0.1M\right)}{0.093M + \left(0.1M\right)}$$

$$v = 0.0006151\ M \bullet s^{-1}$$

2.3 Results and Discussion[42]

2.3.1 Overall Pump Design

Enzymes have been demonstrated to move by generating a continuous surface force in fluid.[6] Therefore, immobilizing the enzymes on a patterned surface should allow them to function as a micropump, moving the surrounding fluid in a directional manner. Four different enzymes were initially used to characterize this analyte-specific fluid pump. The enzymes examined were catalase, urease, glucose oxidase, and lipase. The selected enzyme was immobilized on an Au-patterned surface as described in Section 2.2.1. Sulfate-functionalized polystyrene microspheres were used as tracer particles to aid in tracking of fluid flow.

A hybridization chamber, also known as a spacer, was placed on top of the enzyme patterned surface, in order to contain the necessary substrate and tracer particles for analysis. A buffered solution of substrate with suspended polystyrene tracer particles was then injected into the sealed chamber placed upon the Au patterned surface. This assembly was then monitored using the microscope setup described in Section 2.2.2.

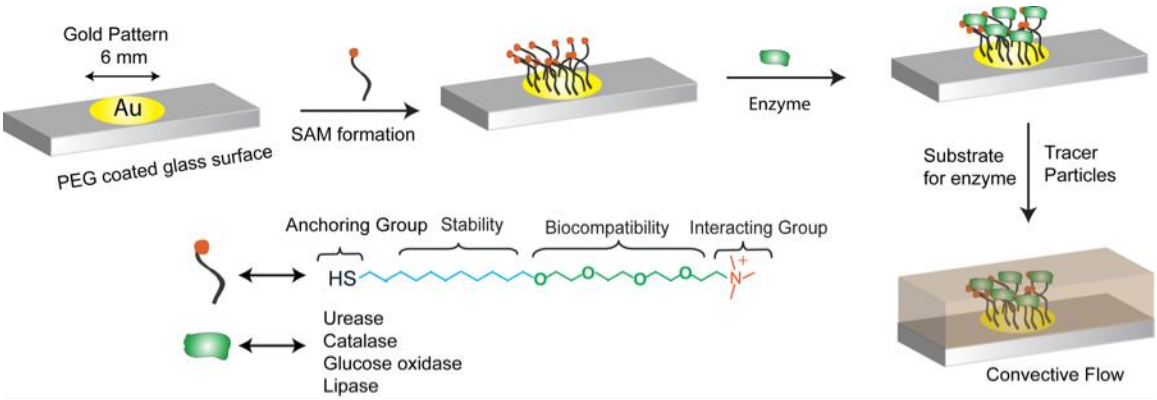

Figure 2-2: Schematic of gold-patterned surface functionalized with linker and enzyme in a fluid-filled chamber

2.3.2 Determination of Site-Selective Enzyme Immobilization

It was necessary to ensure that the enzyme was selectively functionalized only to the Au-pattern on the glass slide, in order to control any pumping effects associated with loose enzyme. To accomplish this, the Au-patterned PEG-coated glass slide was incubated with fluorescently labeled enzymes. The surface was then viewed under a fluorescence microscope in the presence of buffer, and it was determined that no fluorescence signal was observed on the PEG-coated glass surface. The enzyme was successfully localized to the evaporated Au pattern. This is demonstrated by the following figure.

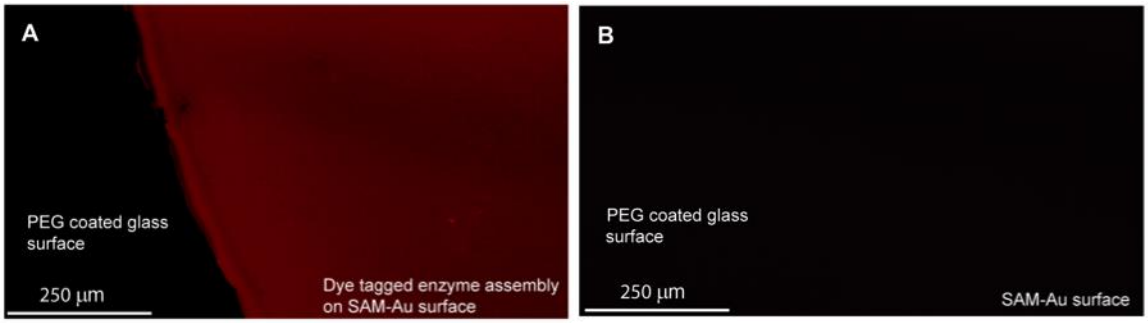

Figure 2-3: Fluorescent image of SAM-modified Au surface in presence of fluorescently-tagged enzyme

2.3.3 Catalase-Functionalized Enzyme Micropump

As a near kinetically-perfect enzyme, catalase was an ideal choice for the first enzyme-powered micropump. Catalase is part of the larger enzyme class of peroxidases, and is widely found in biological systems, dealing with the remediation of toxic hydrogen peroxide into the harmless products of oxygen and water.[17]

As detailed in Section 2.2, the enzyme was selectively immobilized to the Au-pattern on the PEG-coated glass slide using a quaternary ammonium thiol linker. A spacer was placed on

the surface and sealed, such that a solution of buffer with suspended polystyrene microspheres and a chosen concentration of the enzyme's respective substrate could be injected into the chamber. When viewed under the microscope, the tracer particles were shown to move towards the Au pattern, when viewed approximately 30 μm from the surface. When viewed significantly above the Au pattern, due to the nature of a closed system, the particles were shown to be moving away from the pattern, due to fluid continuity. A substrate-concentration-dependent model was first investigated, by using various concentrations of hydrogen peroxide. The concentrations tested were 0.001 M, 0.01 M, 0.05 M, and 0.1 M. The tracked speeds of the polystyrene tracers showed an increase in speeds as concentration increased. A control was conducted in the absence of substrate, where it was predicted and confirmed that no fluid movement would occur. Pumping velocities increased from 0.37 μm in 0.001 M substrate to 4.51 μm/s in 0.1 M substrate.

Substrate Concentration (M)	**Reaction Rate (μM/s)**	**Pumping Speed (μm/s)**
0.001	12.60	0.371 ± 0.067
0.01	115.0	0.653 ± 0.129
0.05	414.0	2.20 ± 0.28
0.1	613.5	451 ± 0.35

Table 2-1 : Substrate concentration dependent pumping of catalase powered micropump

The error bars in Figure 2-4 denote the standard deviations for each pumping velocity measured, as indicated in Table 2-1. The literature value of k_{cat} used to calculate the reaction rate was 2.12 x 10^5 s^{-1}. The literature value of K_M used in the calculation was 0.093 M. The enzyme was known to have four active sites.[18,19] In order to determine the pumping velocity at each substrate concentration, 30 tracer particles were tracked, and the mean of each individual

pumping velocity was calculated. The differences between the pumping velocities at varying concentrations of substrate were found to be statistically significant, with a P value less than 0.01.

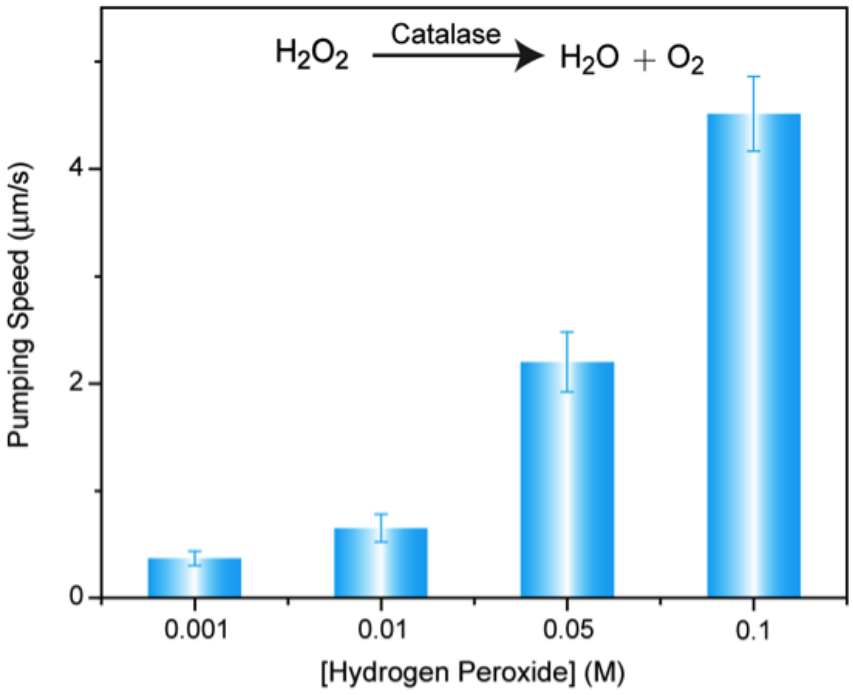

Figure 2-4 : Pumping velocities for catalase powered micropump at various concentrations of hydrogen peroxide

2.3.4 Urease-Functionalized Enzyme Micropump

Urease is part of the class of enzymes known as hydrolases. Studies were conducted using this enzyme in a similar manner to those in Section 2.3.3. The enzymes were immobilized using the quaternary-ammonium thiol linker to the Au surface and covered with a spacer into which buffered substrate, urea, was injected. The fluid flow was monitored via tracking of

sulfate-functionalized polystyrene microspheres. Near the enzyme-immobilized Au pattern, the fluid was shown to be pumping outwards, away from the gold patch. When viewed farther up in solution away from the surface, due to fluid continuity, the fluid was viewed in the opposite direction, towards the patch.

As expected from previous trials with catalase, the urease pump also had an increase in pump velocity when urea concentration was increased. Several other concentrations of urea were tested for this enzyme, namely 0.001 M, 0.01 M, 0.1 M, 0.25 M, 0.5 M, and 0.75 M. Higher concentrations of substrate could be used when compared to catalase due to two factors: urease is not kinetically perfect and hence does not catalyze reactions as quickly, and hence does not result in pumping velocities that compare to catalase, and the reaction of urea to amine does not create gaseous bubbles which may cause undesired fluid flows. The pumping velocity increased from 0.24 μm/s in 0.001 M urea to 0.80 μm/s in 0.75 M urea. The data table comparing the average speeds with calculated reaction rates is shown below, along with the graph showing the increase in pumping velocity as substrate concentration increased.

Substrate Concentration (M)	Reaction Rate (μM/s)	Pumping speed (μm/s)
0.001	44.83	0.235 ± 0.046
0.01	91.25	0.342 ± 0.092
0.1	101.8	0.404 ± 0.093
0.25	102.6	0.464 ± 0.088
0.50	102.8	0.622 ± 0.117
0.75	102.9	0.797 ± 0.125

Table 2-2 : Substrate concentration dependent pumping of urease powered micropumps

The error bars in Figure 2-5 denote the standard deviations for each pumping velocity measured, as indicated in Table 2-2. The literature value of k_{cat} used in the calculation was 23000 s^{-1}, while the literature K_M was 0.0013 M. The enzyme molecule was known to have six active

sites.[19] A total of 30 tracer particles were tracked for each substrate concentration, and each individual tracer particle velocity was summed and averaged to gain a total average pumping velocity for that substrate. The differences between each pumping velocity were found to be statistically significant, with a P value less than 0.01.

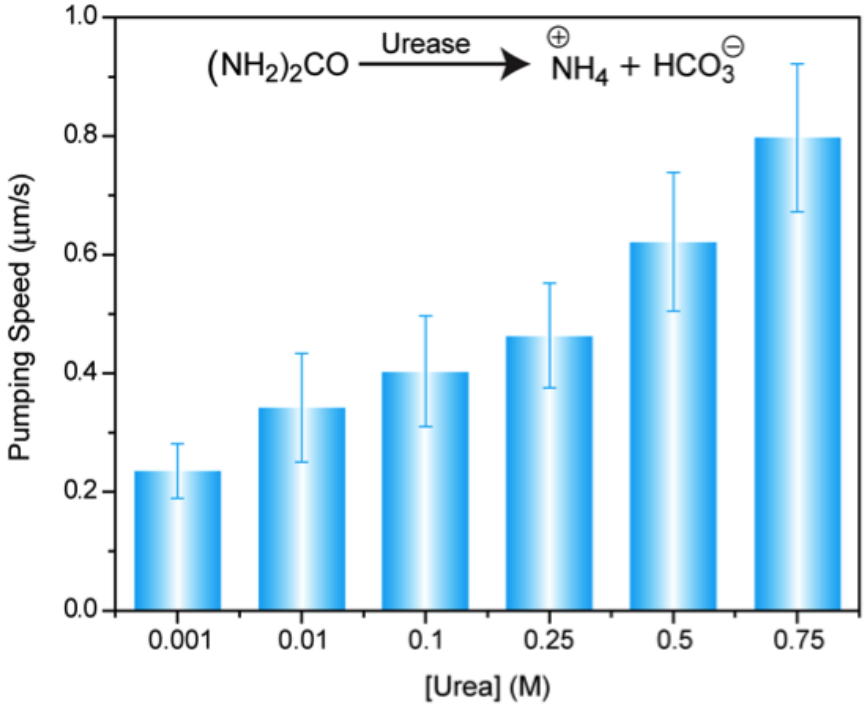

Figure 2-5 : Graph of pumping velocities for urease powered micropump at various concentrations of urea

2.3.5 Lipase-Functionalized Enzyme Micropump

Lipase is an enzyme that belongs to the class of esterases. It is used in the human digestive tract in the breaking down and processing of lipids such as triglycerides, fats, and oils.[20] Studies conducted with lipase were done in a similar manner to that which was described with the other enzyme systems. The enzyme was immobilized via the quaternary-ammonium thiol linker on the Au-patterned PEG-coated class slide. A chamber was fitted and sealed on top

of the assembly, into which a buffered solution of substrate (4-nitrophenyl butyrate) was injected, along with suspended sulfate-functionalized polystyrene microspheres.

When viewed close to the immobilized-enzyme Au surface, the fluid was noted to be moving towards the pattern, pumping inwards. Farther up in solution, in accordance with fluid continuity, it was observed that the fluid was moving away from the pattern. As predicted, the pumping velocity increased in direct relation with the substrate concentration. In this study, 4-nitrophenyl butyrate (PNB) was used in concentrations of 0.001 M, 0.01 M, 0.1 M, and 0.5 M. The pumping velocity increased from 0.27 μm/s in 0.001 M PNB to 0.54 μm/s in 0.5 M PNB. The calculations of reaction rate for each substrate concentration along with the pumping speeds are shown in the table below, as well as graphically in the following figure.

Substrate Concentration (M)	Reaction Rate (μM/s)	Pumping Speed (μm/s)
0.001	0.01706	0.269 ± 0.068
0.01	0.02311	0.347 ± 0.090
0.1	0.02396	0.400 ± 0.091
0.5	0.02404	0.541 ± 0.106

Table 2-3 : Substrate concentration dependent pumping of lipase powered micropumps

The error bars in Figure 2-6 denote the standard deviations in pumping speed, as denoted in Table 2-3. The literature value of k_{cat} used in this calculation was 5.08 s^{-1} while the literature value of K_M was 0.00041 M. The enzyme molecule was assumed to have 1 active site.[21] A total of 30 tracer particles were tracked for each substrate concentration, and their individual velocities were averaged to give the overall average pumping speed. Statistical data showed that there was a significant difference between pumping speeds at each of the concentrations tested, as denoted by a P value of less than 0.01.

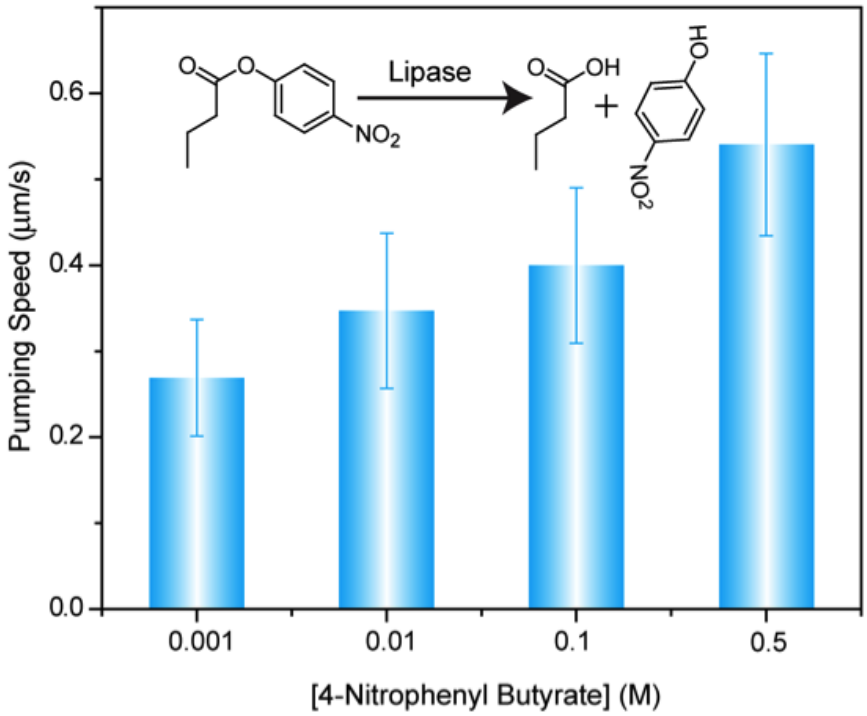

Figure 2-6 : Graph of pumping velocities for lipase-powered micropump at various concentrations of 4-nitrophenyl butyrate

2.3.6 Glucose Oxidase-Functionalized Enzyme Micropumps

Glucose oxidase is a member of the oxidases, another family of enzymes. It is used in the body to help break down sugar in cells into various metabolites. The body also uses glucose oxidase to monitor glucose concentration that is freely available in blood plasma, and has been used as a biosensor in nanotech applications.[22] Experiments conducted using glucose oxidase employed a method similar to those of the experiments conducted with other enzymes. The glucose oxidase enzyme was immobilized to the Au-patterned PEG-coated glass slide using the quaternary ammonium thiol linker via an electrostatic assembly. A spacer was placed on top of this assembly and sealed, into which a solution of buffered substrate was injected, along with sulfate-functionalized polystyrene microparticles.

In experiments involving glucose oxidase, the solution of varying concentrations of substrate was first saturated with oxygen by bubbling oxygen through buffer prior to beginning experiments, as oxygen is necessary for the reaction to proceed to completion. As with other trials of enzymes, when viewed close to the Au-patterned surface, the particles were shown to be moving inwards, indicating that the enzymes were pumping in. When viewed farther up in solution, away from the pattern, by fluid continuity the particles were moving away from the pattern, revealing convective flow. The concentrations of glucose that were tested in this experiment were 0.001 M, 0.01 M, 0.1 M, and 1 M. As expected, the pumping velocity increased with increasing substrate concentration. The velocities increased from an average of 0.24 μm/s in 0.001 M glucose to 0.79 μm/s in 1 M glucose. The pumping velocities in relation to substrate concentration are shown in the table below, and graphically represented in the following figure.

Substrate Concentration (M)	Reaction Rate (μM/s)	Pumping Speed (μm/s)
0.001	0.02937	0.239 ± 0.083
0.01	0.2276	0.330 ± 0.055
0.1	0.7004	0.411 ± 0.081
1	0.8841	0.790 ± 0.117

Table 2-4 : Substrate concentration dependent pumping of glucose oxidase powered enzyme micropump

The error bars in Figure 2-7 denote the standard deviations for each concentration dependent pumping velocity, as denoted in Table 2-4. To calculate the reaction rates for glucose oxidase at each substrate concentration, literature values for the k_{cat} and K_M were used. The literature value for k_{cat} was found to be 920 s^{-1}, while the literature value of K_M was found to be 0.030 M. The enzyme was found to have two active sites.[23] To determine pumping speeds at each substrate concentration, 30 particles were tracked, their individual velocities being summed

and averaged to gain the average pumping speed. The differences in pumping velocities for each substrate concentration were statistically distinct, with a P value of less than 0.01.

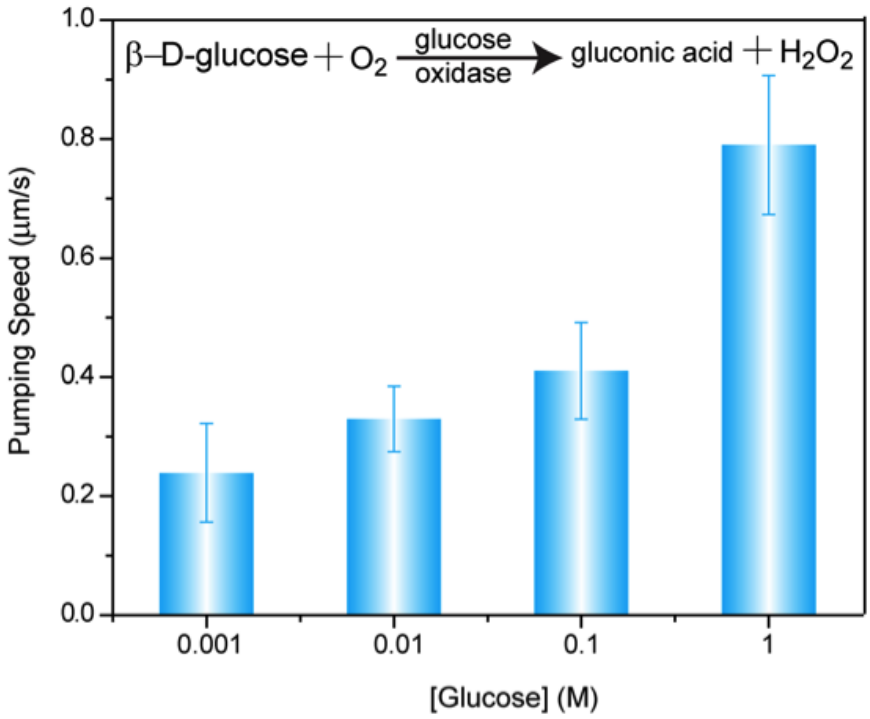

Figure 2-7 : Graph of pumping velocities for glucose oxidase powered micropumps

2.3.7 *In Situ* Analyte Triggered Pumping

From previous experiments it was shown that the enzyme-powered micropumps have the ability to detect specific analytes in their surroundings, and cause pumping in a concentration dependent manner. This property makes these pumps ideal for being used as sensors and pumps. To this effect, catalase enzyme was immobilized to the gold pattern in a similar manner as described above, covered with a spacer, and sealed. Rather than injecting a buffered solution of hydrogen peroxide (catalase's substrate), substrate was generated *in situ* by the injection of glucose oxidase and glucose in oxygenated buffer. The concentration of glucose tested was 50

mM, which was a previously tested result. The conversion of glucose to gluconic acid and hydrogen peroxide would provide substrate for the catalase pump, from which pumping could then be observed. It was shown that under these conditions, fluid was observed to be pumping inwards near the pattern, at a rate of 1.2 μm/s.

It was also shown that pumping was not shown in the absence of glucose oxidase, or glucose alone, or both. This demonstrates that these pumps can be specific to certain analytes and can act as detectors and pumps. A schematic showing the experimental setup is shown below, where the catalase enzyme is immobilized on the gold pattern on the PEG-coated glass slide surface, and covered with a spacer that is filled with buffer, glucose oxidase, and glucose. Upon addition of the solution, pumping is observed in the inwards direction.

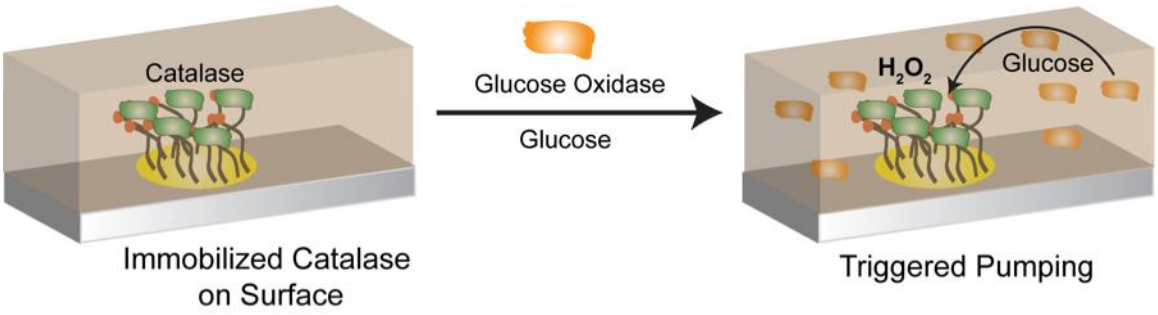

Figure 2-8 : Schematic of immobilized catalase in a solution of glucose oxidase and glucose for *in situ* generation of hydrogen peroxide to achieve fluid pumping

2.3.8 Temporal Variations in Pumping Velocity in Enzyme Pump Systems

In each of the four enzyme pump systems, the temporal regulation of pumping speeds was investigated. The viability and any variations in pumping velocities were aimed to be determined over both short and long time scales. Catalase was the first system tested, using three different concentrations of substrate on a short-term time scale. Studies were conducted similarly to those described above, with the enzyme being immobilized to the Au-patterned PEG-coated

glass slide, which was then covered with a sealed spacer and injected with a buffered solution of substrate and sulfate-polystyrene microparticles. The concentrations of substrate (hydrogen peroxide) tested were 10 mM, 50 mM, and 100 mM, and each study was conducted for eleven minutes. The graph of the variation in pumping speeds for the 10 mM and 100 mM trials are shown below.

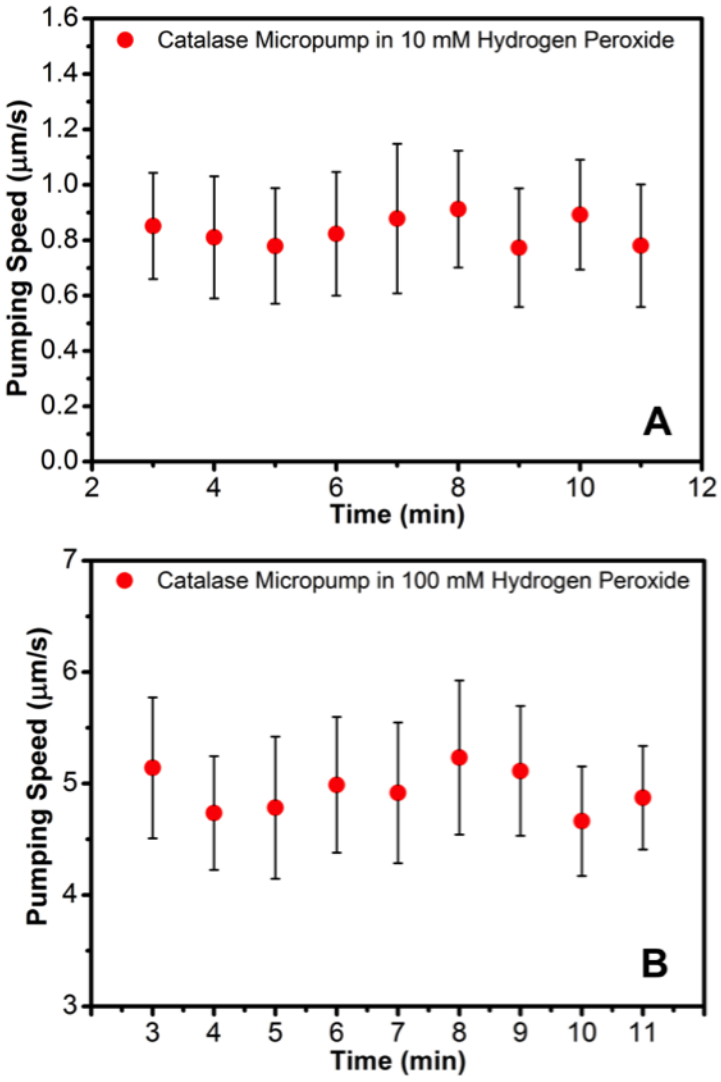

Figure 2-9 : Graph of short-term variation in catalase pumping velocities over short times

The error bars in the above figure denote the standard deviations in pumping velocity. As shown in the graph, there was no significant deviation in pumping velocities observed over the

short-term. The statistical analysis gave a P value greater than 0.01 for the differences between the time periods, indicating that there was no real change in pumping velocities.

This temporal characterization of the enzyme pump system was then explored for the other enzyme systems of interest, namely urease, lipase, and glucose oxidase. Only one concentration of substrate was tested for each of these enzyme systems. For urease, the experiment was conducted using 0.75 M urea, 1 M glucose for glucose oxidase, and 0.5 M 4-nitrophenyl butyrate for lipase. The results below show the variations in pumping speeds for each of the enzymes, including the 50 mM hydrogen peroxide trial of catalase.

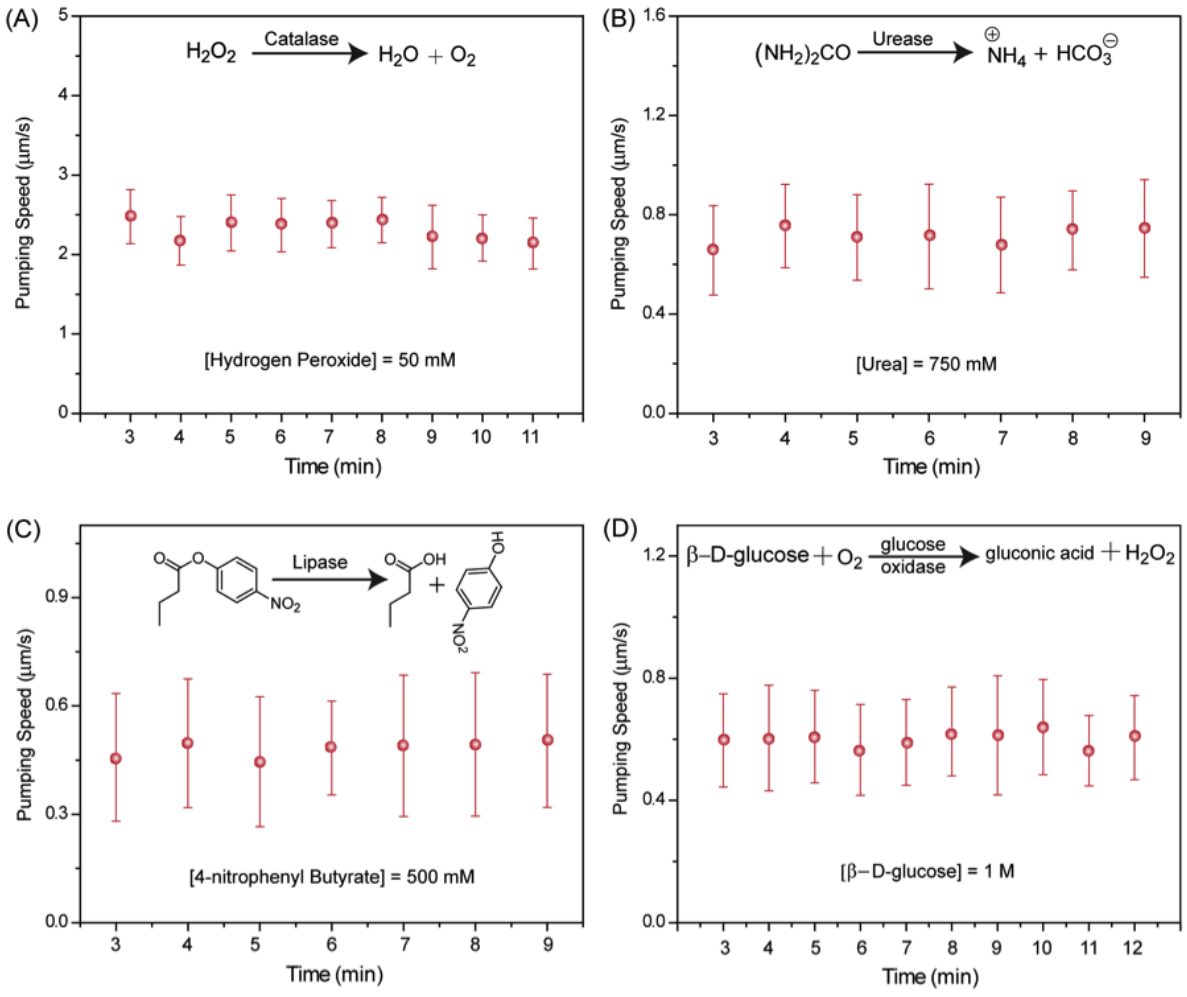

Figure 2-10 : Graph of variations in pumping velocities for each of the four enzyme micropumps over short times

The error bars in the above figure denote standard deviations for each time point. The statistical analysis showed that there was not a significant difference between time points for each respective enzyme system ($P > 0.01$), and hence it was determined that in this time period the pumping velocity does not significantly differ from one point to the next. This thereby affirms that these enzyme-powered micropumps are robust enough to function for longer periods of time.

To further investigate the true viability of these enzyme micropumps, their performance in long-term temporal studies was also examined. For this trial, experiments were conducted using the urease enzyme pump system. The goal of this study was to determine how long the pumps could generate directional fluid flow at a rate similar to that at which they began, and what was the nature of their decrease in pumping velocities. The urease system was monitored over a period of 210 minutes, where it was determined that it was sufficiently close to the zero point of pumping to stop. The graph of this data is shown below.

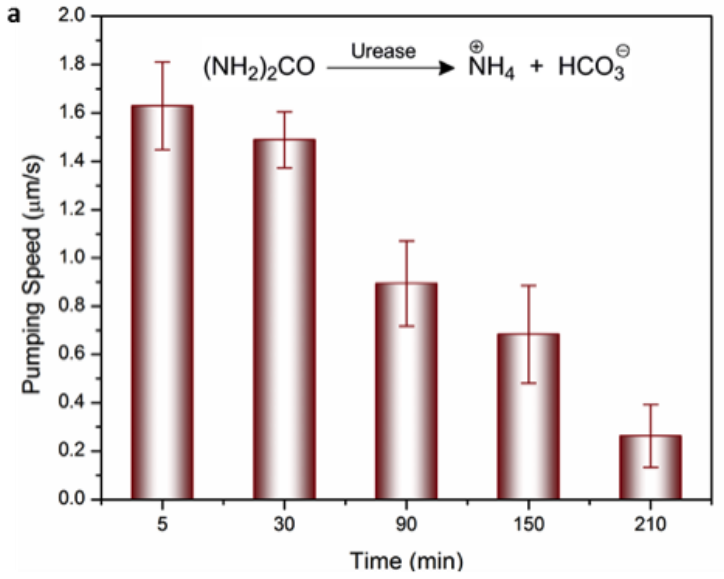

Figure 2-11 : Pumping velocities for long-term study of urease powered micropump

The error bars in the above figure denote standard deviations for each data point. As was shown in the previous experiment with the short-term temporal study, at the five minute data point the pumping velocity for urease was largely unchanged. Surprisingly, the pump maintained its directed fluid velocity fairly consistently up to 30 minutes. The pump began to decrease in velocities around 90 minutes, but continued to show directional fluid flow all the way to 210 minutes. This proved that the system is extremely robust and viable for a very long period of time, increasing its potential applicability and uses.

Having determined the long-term viability of the enzyme-micropump in one of our enzyme systems, the ability to restore the pump velocity to its original pumping speed was explored. This was accomplished by introducing fresh substrate for the enzyme into the chamber, long after the original substrate had been run and the pump velocity had sufficiently decreased.

To test this theory, two different enzyme systems were used. One was the catalase enzyme system, with 0.5 M hydrogen peroxide substrate. The second system was the urease system, using 1.0 M urea. More data points were recorded for the catalase system to better characterize the nature of the decrease in speeds. After a sufficient amount of time had passed for the pump velocity to have significantly decreased, the spacer was removed from the enzyme-micropump assembly and the solution was removed and dried from within the spacer. Then, a new spacer was sealed atop the Au-patterned slide, and fresh substrate solution with tracer particles was injected into the assembly. The results for this experiment are shown graphically below.

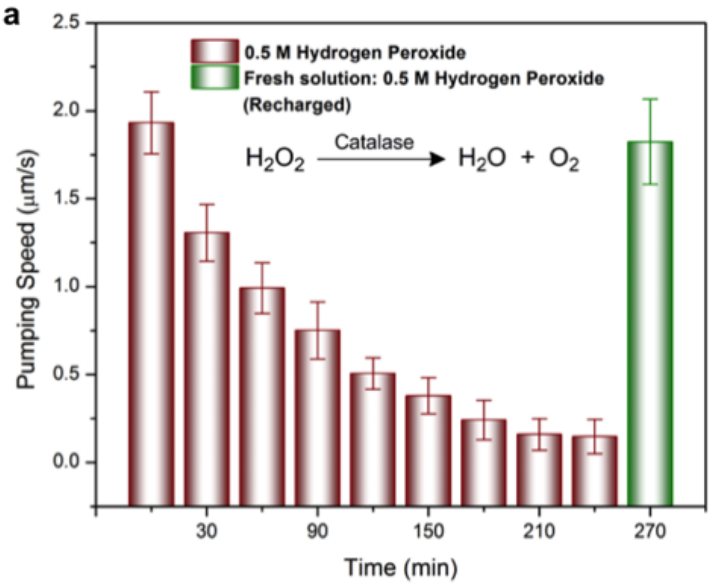

Figure 2-12 : Graph of long-term study of catalase powered micropump with recharging

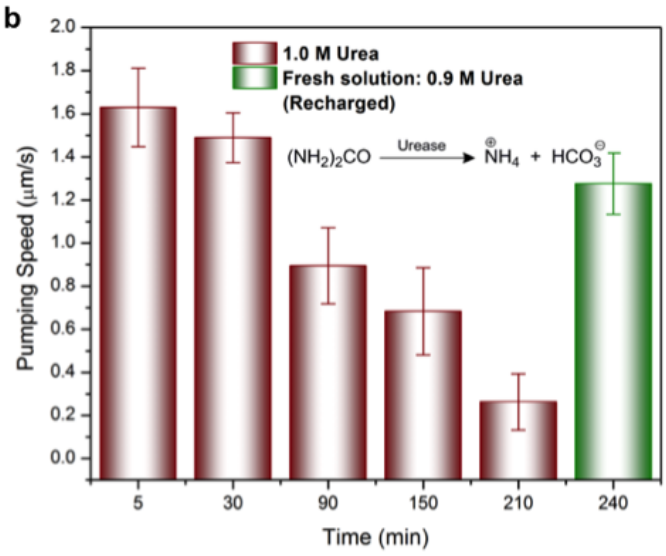

Figure 2-13 : Graph of long-term study of urease powered micropump with recharging

Error bars in the above figures denote the standard deviations for each data point. As can be seen in the graphs in the above figures, the recharging of the pumps with fresh substrate tended to increase the pumping velocity back near the initial value obtained for pumping, demonstrating that the enzymes were still viable after a long period of time. This also helped

determine that the decrease in pumping speeds observed in the extended temporal study was likely due to the decreasing concentration of substrate as the enzyme-substrate system reached equilibrium, rather than any changes in the catalytic activity of the enzymes.

2.3.9 Spatial Variations in Pumping Velocities in Enzyme Micropumps

Early studies were conducted by observing the edge of the enzyme-functionalized Au-pattern. To determine the effects of fluid pumping farther away from the pattern, videos were recorded at several different distances from the Au-pattern. Due to the nature of fluid pumping in microscale systems (low Reynolds number systems), the velocity of the tracer particles at distances farther from the pattern would also have to be due to active pumping by the enzyme, rather than bulk fluid movement.

Due to the time consuming nature of the experiments themselves, there was a slight temporal delay in recording videos at varying distances from the pattern. However, as in the above Section 2.3.8 it was established that pumping speeds were generally consistent until approximately 30 minutes into the experiment, it was determined that the pumping speeds would not vary considerably due to the temporal aspect of the study, and instead any variations determined would be a result of a spatial component.

The four enzyme systems were tested at a single concentration of substrate without recharging, in that they were not re-injected with fresh substrate. The enzyme of interest was selectively immobilized to the Au-pattern on the PEG-coated glass slide via an electrostatic assembly facilitated by the quaternary ammonium thiol linker. A spacer was sealed on top of the area surrounding the Au-pattern, into which a buffered solution of substrate with sulfate-

functionalized polystyrene microspheres was injected. The concentrations of substrate tested were 10 mM hydrogen peroxide for catalase, 1 M urea for ureas, 1 M glucose for glucose oxidase, and 0.5 M 4-nitrophenyl butyrate for lipase. The graph of pumping velocities is shown below.

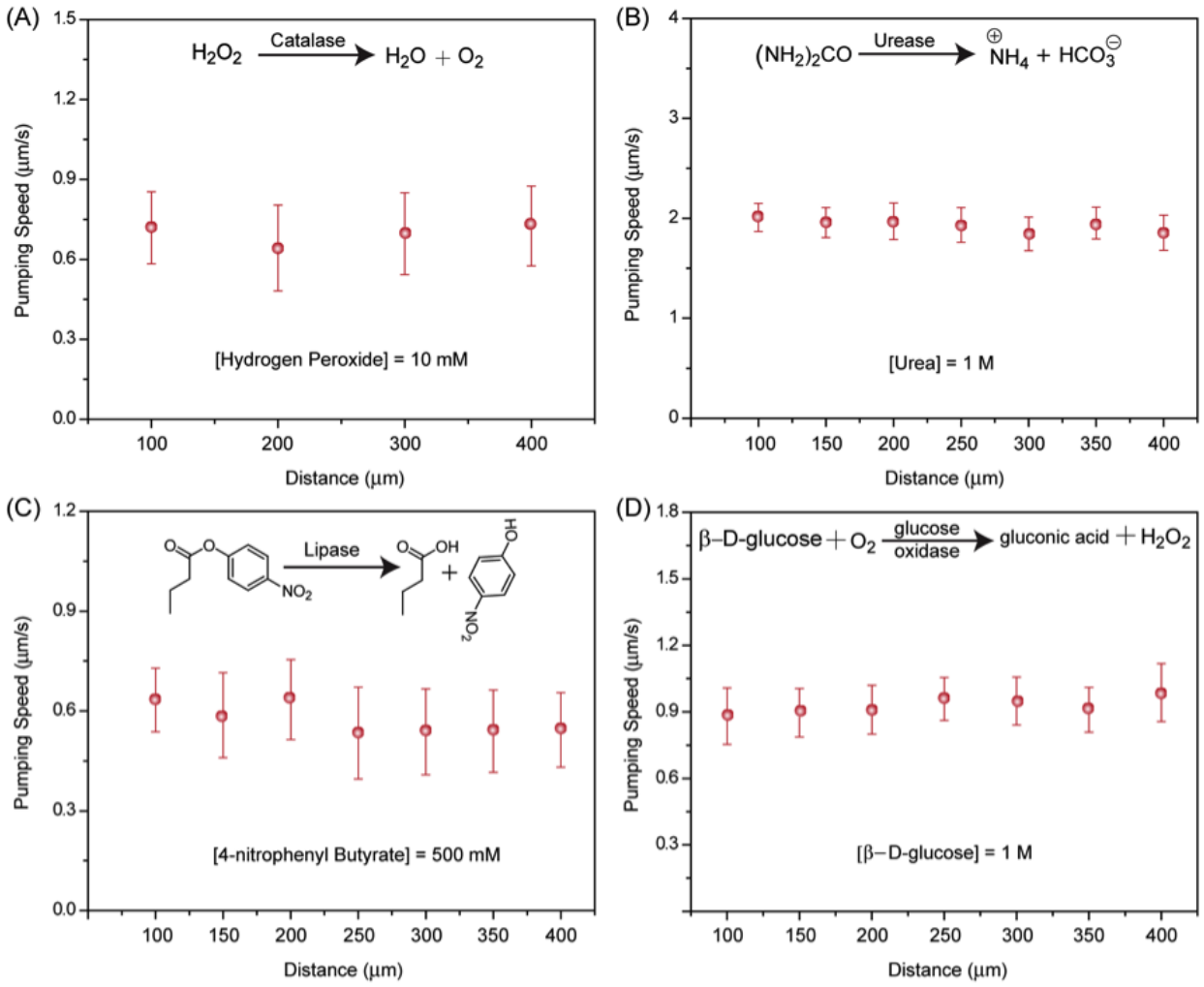

Figure 2-14 : Spatial dependent pumping for four different enzyme micropump systems

The error bars in the graph above denote standard deviations for each individual data point. Each pumping velocity was determined by tracking 30 tracer particles in solution. As can be seen from the graphs above, none of the enzyme systems displayed a significant difference in pumping velocities as the viewing frame was moved away from the pattern. This demonstrates

the ability of the pump to effect fluid flow over relatively large distances and increases its potential applications.

2.3.10 Determination of Fluid Pumping Mechanism

The experiments described above generated a data set that well characterized the nature of the functionality of these enzyme micropumps. It was shown that they increased their pumping velocity in relation to increasing substrate concentration, that they remained stable in pumping velocities throughout both spatial and temporal assays, and that they could be adequately recharged with fresh substrate. However, this does not shed light on the limits of the micropumps concerning reactive sensing and detection limits for certain analytes. For this reason, further experimentation and modeling was conducted in order to determine the true mechanism of fluid pumping exhibited by the enzyme micropumps. A number of theories described in Chapter 1 were considered, and many were ruled out as experiments were conducted.

2.3.11 A Possible Mechanism: Non-Electrolytic Diffusiophoresis

A catalyst affixed to a surface can, in the presence of substrate, lead to the production of two asymmetric products. In the case of these enzyme pumps, the biological catalyst can generate two different solutes from one substrate, developing a gradient of solutes in the present solution. The catalase micropump system does not generate charged species from the degradation of hydrogen peroxide, thus making the mechanism of this pumping a possible

candidate for non-electrolytic diffusiophoretic pumping. In the catalase micropump system, the directional movement of tracer particles could be considered a result of non-electrolytic diffusiophoresis, where the breakdown of hydrogen peroxide to water and oxygen creates a gradient of solutes. This effectively generates more molecules in the vicinity of the enzyme pattern, generating an density related osmophoretic force around the pattern.

In order to test this theory, an assay was developed whereby the entire pump setup was inverted on the microscope stage. If non-electrolyte diffusiophoresis was the major pumping mechanism at play, this experiment should have resulted in the tracer particles being observed to move in the same direction as in previous trials, towards the pattern. However, such an experiment resulted in tracer particles close to the Au-pattern moving in the opposite direction, away from the pattern. By fluid continuity due to the nature of the closed spacer system, fluid farther away from the pattern was observed to be moving towards the Au-pattern. Since the direction of fluid flow changed upon inversion of the pump system, non-electrolytic diffusiophoresis could not have been the major pumping mechanism.

2.3.12 A Possible Mechanism: Electrolytic Diffusiophoresis

Urease, lipase, and glucose oxidase powered pumps may all be considered candidates for an electrolytic diffusiophoretic mechanism, due to their production of charged solutes. In order to test this theory, trials were conducted using an inverted setup similar to that discussed above. The immobilized enzymes were covered with sealed spacers into which a buffered solution of substrate and tracer particles were injected, and these pumps were then turned upside down on

the microscope stage. If electrolytic diffusiophoresis were the major mechanism of pumping, the direction of fluid flow should remain unchanged for each of these pump systems.

However, the experiments concluded that for each enzyme micropump system, the direction of tracer particles reversed upon inversion. In the urease micropump, the tracer particles close to the Au-pattern were observed to be moving inwards, opposite to the upright scenario. In both lipase and glucose-oxidase powered micropumps, the tracer particles close to the surface were observed to be moving away from the pattern, opposite to their normal condition. In each of these systems, by fluid continuity the direction of tracer particles further reversed when viewed farther away from the pattern. These experiments helped to rule out electrolytic diffusiophoresis as a possible pumping mechanism for these enzyme-powered micropumps.

In order to further corroborate these results, another method of determining if electrolytic diffusiophoresis was at play was employed. The zeta potential of tracer particles has a significant effect on electrolytic diffusiophoresis. The direction of movement should be different when positively versus negatively charged tracer particles are used, if this is the pumping mechanism. The negatively charged sulfate-functionalized polystyrene microparticles employed in previous trials moved towards the pattern for lipase, glucose oxidase, and catalase systems, and moved away from the pattern for the urease system. Placing the opposite charge on the tracer particles by using an amine-functionalized polystyrene microparticle with a positive charge should change the direction of tracer particle movement.

However, in the actual trials conducted with the enzyme pump microsystems, no such reversal in the direction of tracer particles was observed. The direction of fluid pumping was determined to be the same when monitored by amine-functionalized tracer particles as it was

when monitored by sulfate-functionalized tracer particles. The speed of the fluid pumping was also determined to be similar for both amine-functionalized and sulfate-functionalized tracers. The data is graphically represented in the below figure.

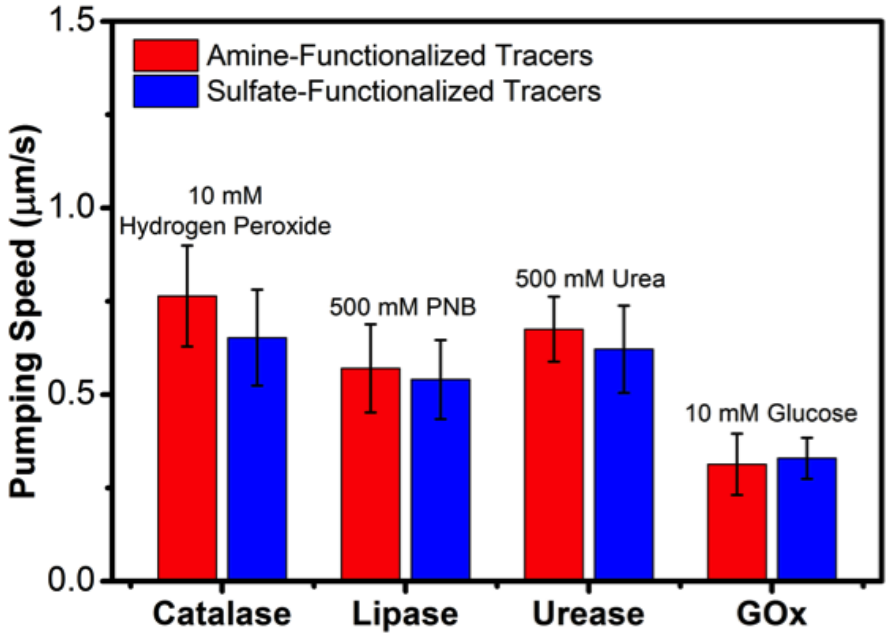

Figure 2-15 : Graph of pumping velocities in each enzyme micropump with amine-functionalized and sulfate-functionalized polystyrene microsphere tracers

As can be seen from the above figure, the pumping velocities remained consistent despite the change from amine-functionalized to sulfate-functionalized tracer particles. The error bars denote standard deviations for each of the enzyme micropump systems. Concentrations of substrate tested are denoted above as 10mM hydrogen peroxide for catalase, 500 mM p-nitrophenyl butyrate for lipase, 500 mM urea for urease, and 10 mM glucose in oxygenaged buffer for glucose oxidase. The error bars and statistical analysis revealed that there was no significant difference in pumping velocities between amine and sulfate-functionalized tracer particles, with a P value less than 0.01.

2.3.13 A Possible Mechanism: Buoyancy-Driven Convection

Aside from ruling out the electrolytic and non-electrolytic diffusiophoretic mechanisms, the inverted pump experiments helped point towards another possible mechanism of fluid pumping, namely buoyancy-driven convection. This is markedly possible due to the exothermic nature of each of our reaction systems, causing the system to release heat as it reacts. This increases the temperature of the liquid directly adjacent to the Au-pattern, decreasing the local density and giving rise to thermally driven convection.

This thermal convection causes flow to be directed upwards from the surface in an upright device. Due to fluid continuity, the fluid flow near the glass surface is hence observed as moving towards the Au pattern. This mechanism further explains the change in fluid flow direction when the pump was inverted, as the lighter fluid attempts to occupy the upper layers and spreads along the glass surface, away from the Au pattern.

This mechanism seems to well-fit the observed behavior of the majority of the enzyme micropumps, however it does not completely explain the behavior of the urease-powered micropump, which pumped fluid in the opposite direction of the other enzyme systems. In the urease system, the catalytic reaction is still exothermic, but the pumping is viewed outwards from the pattern. For this reason, given the ionic nature of the hydrolyzed products of urea, the solvated ions created could in fact increase the density of the fluid near the enzyme pattern. This local increase in density would cause the fluid to spread along the glass surface, giving rise to a buoyancy-driven thermal convective flow that instead resulted in fluid flow away from the pattern. In the inverted trial, the dense fluid created on top of the Au pattern settles to the lower part of the cavity, and fluid continuity drives the fluid flow inwards near the Au patterned glass surface.

To further corroborate these results and validate the pumping mechanism, the velocity of fluid flow was monitored in each of the enzyme micropumps using an inverted system. The pumping speeds determined for the inverted pumps were fairly consistent with what was observed for the up-right setup. This further confirms the buoyancy-driven mechanism of fluid pumping, as the only thing that should have changed when the pump was inverted was the direction of fluid flow. The results of this data are graphically represented in the below figure.

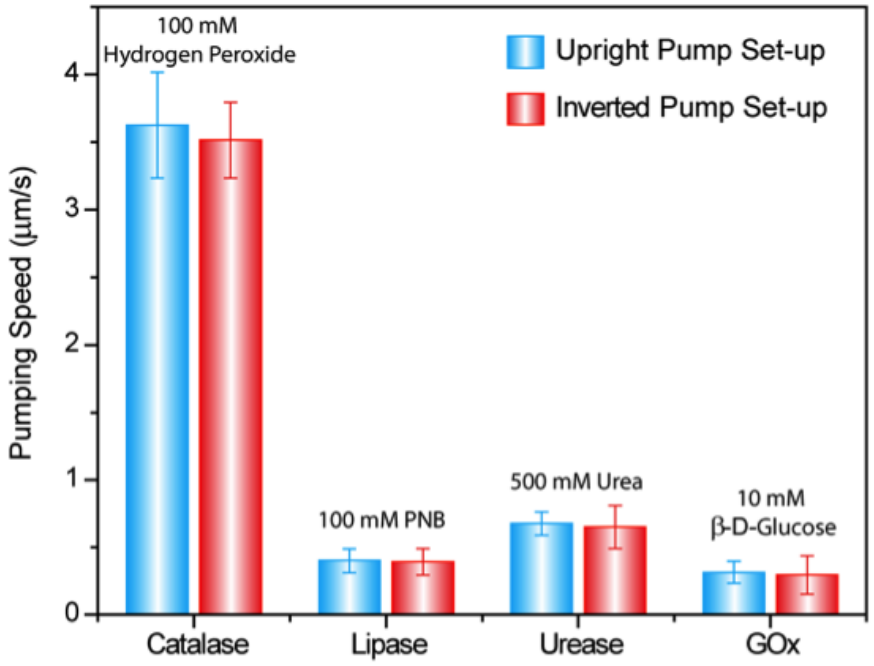

Figure 2-16 : Pumping velocities for each enzyme micropump system in both an upright and inverted setup

Given this mechanism of fluid pumping, it becomes possible to draw some theories from mathematical modeling. The Rayleigh number, R_a gives the intensity of thermal convective flow within a horizontal layer of fluid in the presence of a temperature gradient.

$$R_a = \frac{g\beta h^4}{\nu c}\frac{dT}{dx}$$

Here, g gives the gravitational acceleration, while β gives the coefficient of thermal expansion, h represents the thickness of the liquid layer, ν represents the kinematic viscosity, and χ represents the heat diffusivity of the liquid. The temperature gradient $\frac{dT}{dx}$ can be approximated by determining the heat flux Q (J cm^{-2} s^{-2}), which further depends on the rate and enthalpy of the reaction.

If it is assumed that the flow is steady and small in magnitude, then the speed can be approximated by the following equation.

$$V : \frac{c}{h} R_a f(a)$$

Here, f(a) depends on the geometry of the micropump, where the radius of the pump is R. This allows us to express f(a) as a function of the ratio R/h. Further, if r is the rate of the reaction and ΔH is the enthalpy of the reaction, then we can approximate the heat flux using these parameters. This equation is shown below.

$$Q = \frac{r \Delta H}{\rho R^2}$$

Thus, we can get a more detailed picture of the flow velocity by manipulating the above equations. This overall equation for the pumping velocity is given below.

$$V : \frac{g \beta h^3 r \Delta H}{\nu \kappa \rho R^2} f\left(\frac{R}{h}\right)$$

In this equation, κ denotes the thermal conductivity of the fluid. This equation also gives the dependence of thermally driven flow on the thickness of the liquid layer and negates the influence of other microscopic phoretic processes, where the speed is independent of thickness.

The above equation gives the relationship between the speed of fluid pumping and the thickness of the liquid. At a given height (h), for a fixed radius (R), the magnitude of *f*(a) changes accordingly. This changes the multiplier of the velocity function, thereby changing the pumping velocity. If this model were to be considered correct for the pump system, this would indicate that a change in pumping velocities should be observed when the height of the spacer was increased.

This was experimentally tested using a similar setup to those of previous experiments, using spacers that were double the height as per the original trials. The above equation gives the parameter that *f*(a) has available values from zero up to 10^{-3}, and saturates beyond a value of d > 2h. Given this parameter, an increase in *h*, the layer thickness, should result in an increase in the flow speed of h^3. This was experimentally tested by using a spacer with twice the height of the ones used in previous trials, and monitoring the pumping speed in a similar manner. The results of these trials are shown graphically below.

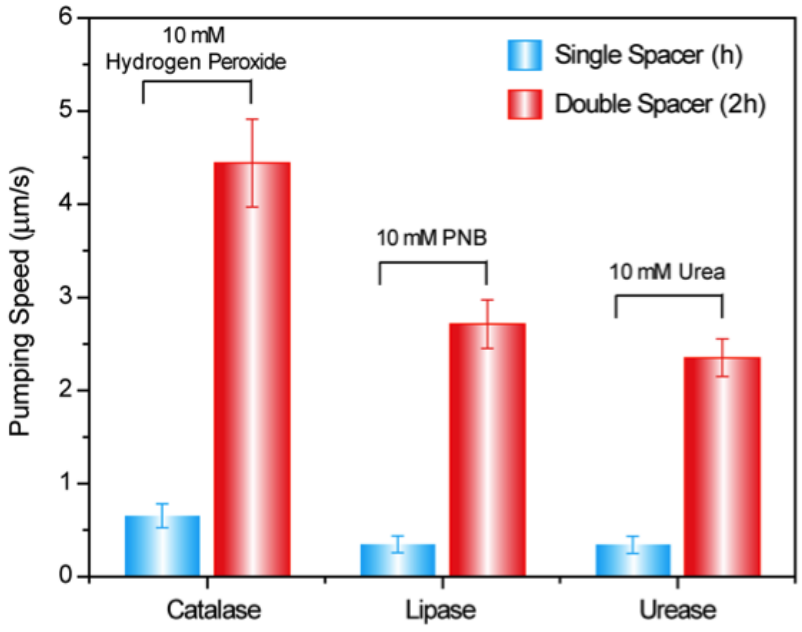

Figure 2-17 : Pumping velocities for single-spacer and double-spacer experiments for a single substrate concentration in different enzyme systems

The graph above displays that the pumping speeds dramatically increased when the spacer height was doubled for each of the enzyme systems tested. Catalase was tested with 10 mM hydrogen peroxide substrate, lipase was tested with 10 mM p-nitrophenyl butyrate substrate, and urease was tested with 10 mM urea substrate. The error bars denote standard deviation for each trial. As was predicted from the mathematical model, the speeds for each enzyme system increased approximately by a factor of eight when the spacer height was doubled, fitting will with the mathematical model. This further confirms this mechanism of pumping action.

2.4 Conclusion

These experiments demonstrated the creation and characterization of the first ATP-independent non-mechanical enzyme powered micropump outside of a biological system. These novel devices were created by immobilizing enzymes onto Au-patterned PEG-coated glass slides. The monitored fluid pumping speeds showed that there was a substrate-concentration-dependent increase in pumping velocities. Additionally, it was displayed that these pump systems could exert spatial and temporal control over fluid transport.

The mechanism behind the pumping of fluid in response to the enzyme being in the presence of substrate was found to be a catalysis-induced buoyancy-driven convective flow. Demonstrating that immobilized enzymes can create a fluid flow autonomously upon reaction with various concentrations of an analyte, and can respond to those concentrations in a smart manner, will allow for the creation of sophisticated devices with specific levels of control over the location and flow rate of fluids and colloids. The observations in this chapter may help enhance microfluidic device design and advance the field as a whole.

Chapter 3 : Enzyme Pump Hydrogel Scaffolds

3.1 Introduction

Hydrogels are polymer networks which contain significant amounts of water, but are not soluble in water.[24] Famous for their biomedical applicability, hydrogels were the first biomaterials that were designed to be used in the human body. Though they are swollen with water, their polymeric structure allows them to maintain a specific three-dimensional structure.[25]

When the field of hydrogel scaffolding began, the traditional methods of creating the structure included crosslinking copolymerization, crosslinking of reactive polymer precursors, and crosslinking via polymer-polymer reactions. However, these traditional methods of hydrogel synthesis resulted in polymers with a high degree of variability in terms of molecular weight and length, and their structure was also difficult to control as a result of side reactions. Additionally, these were relatively slow to respond to specific signals in solution and often displayed poor mechanical properties.[25]

Current methods of hydrogel scaffolding have created a highly diverse set of structures that are useful for a variety of experimental setups, and have many mechanical properties. For instance, superporous hydrogels and self-assembled hydrogels from copolymers are current areas of hydrogel research. These new hydrogels also allow for increased mechanical stability and decreased response times.[25]

Double networks are a type of hydrogel that is formed when two hydrophilic networks are crosslinked, where one is tightly bound and the other is loosely associated. This allows for a hydrogel with significantly improved mechanical properties, giving it enhanced hardness and

toughness. Some of these hydrogels are also stimuli-responsive. These gels will swell or shrink in response to changes in local pH, temperature, ionic strength, electric or magnetic fields, or light.[25]

As a proof-of-concept for the applicability of the concept of enzyme pumps for drug delivery, a hydrogel support for cargo molecules was created in which a positively charged hydrogel scaffold assembly was coated with enzymes by way of electrostatic attachment. As the enzyme-micropump systems had displayed the ability of the enzymes to generate fluid flow at various speeds in a substrate-concentration-dependent manner, it is expected that when placing the scaffolds in varying concentrations of substrate solution, drug molecules can be released on demand due to the flows that arise in the vicinity of the scaffold and penetrate the structure. This allows for the creation of a bio-compatible regulated smart biosensor and pump.

3.2 Experimental Methods

3.2.1 Synthesis of Positively Charged Hydrogels by Co-polymerization[42]

The first monomer, N-isopropylacrylamide (NIPAAm; TCI Chemical) was recrystallized using n-hexane and vacuum dried before use. Another monomer, 2-(Dimethylamino)ethyl methacrylate (DMAEMA; Sigma-Aldrich) was passed through a basic alumina column and stored in a refrigerator prior to use. 1-Chlorobutane, ammonium persulfate (APS), N,N'-methylenebisacrylamide (MBAm), N,N,N',N'-tetramethylethylenediamine (TEMED) were purchased from Sigma-Aldrich. Fluorescein dye was purchased from TCI Chemical and was unmodified prior to use. Chloroform, acetonitrile, and DMSO were purchased from EMD and used unmodified.

The QDMAEMA monomer was synthesized without modification from its established synthetic protocol.[26] 1-Chlorobutane (C4) (2.04 g, 0.022 mol) was added to a solution of DMAEMA monomer (3.12 g, 0.02 mol) in a mixture of acetonitrile (20 mL) / chloroform (10 mL) and heated in an oil bath at 40°C while stirring overnight. The mixture obtained was then added dropwise to cold diethyl ether (200-300 mL) in dry ice to precipitate the product. The precipitate was then filtered and vacuum dried, upon which a ^{1}HNMR spectra was taken (Bruker 400 MHz). ^{1}HNMR (400 MHz, D_2O, ppm): 6.15 (s, 1H), 5.77 (s, 1H), 4.62 (m, 2H), 3.77 (m, 2H), 3.39 (m, 2H), 3.17 (s, 6H), 1.93 (s, 3H), 1.75 (s, 2H), 1.36 (m, 2H), 0.94 (t, 3H). The ^{1}HNMR spectra is shown in Figure 3-18. The values corresponded well with the literature values.

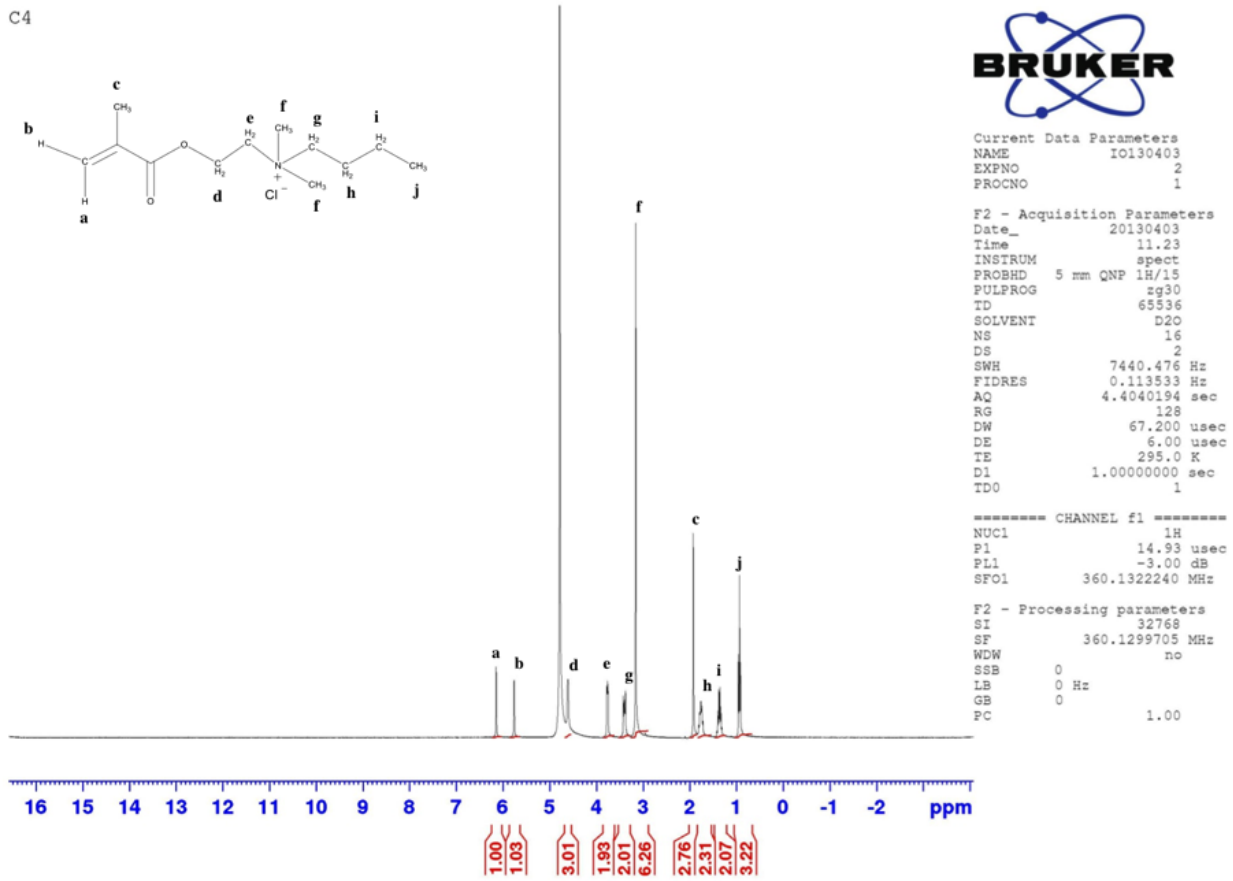

Figure 3-18 : H^{1}NMR spectra of a synthesized QDMAEMA monomer

A free radical polymerization was carried out to copolymerize QDMAEMA-C4 monomer and NIPAAm monomer. This polymerization was conducted in 5 mL H_2O/DMSO (v/v 1:1) mixture at 35°C for approximately 12 hours. QDMAEMA-C4 and NIPAAm were added in a 1:1 feed ratio to the solvent mixture. MBAm was used as a crosslinker and was added to the monomer mixture in a mole ratio of 50:1 total monomers to crosslinker. The polymerization was initiated by APS and accelerated by TEMED. Before adding the initializer, APS (34.2 mg, 0.15 mmol) was diluted in 200 µL of deionized water and added to the monomer mixture, with the simultaneous addition of 0.15 mL of TEMED (3 drops). Once polymerization had occurred, the hydrogel was soaked in deionized water for 120 hours to remove unreacted agents, with the water being changed every six to eight hours. A schematic diagram of this crosslinkage is shown in the figure below.

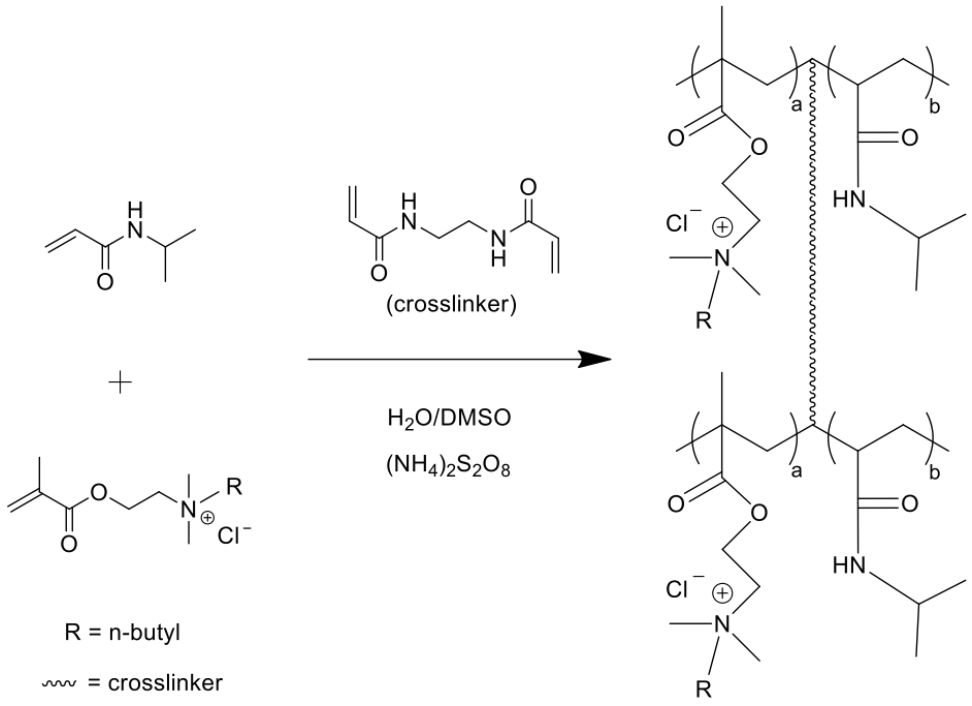

Figure 3-19 : Schematic of the synthesis of polymer hydrogel network via copolymerization of QDMAEMA-C4 and N-isopropylacrylamide

In order to ensure that the crosslinking and gel synthesis had occurred correctly, an FTIR was also run on the gel. The peaks matched well with what was expected in terms of the functional groups on the gel scaffold. The spectra and its annotations are shown in the figure below.

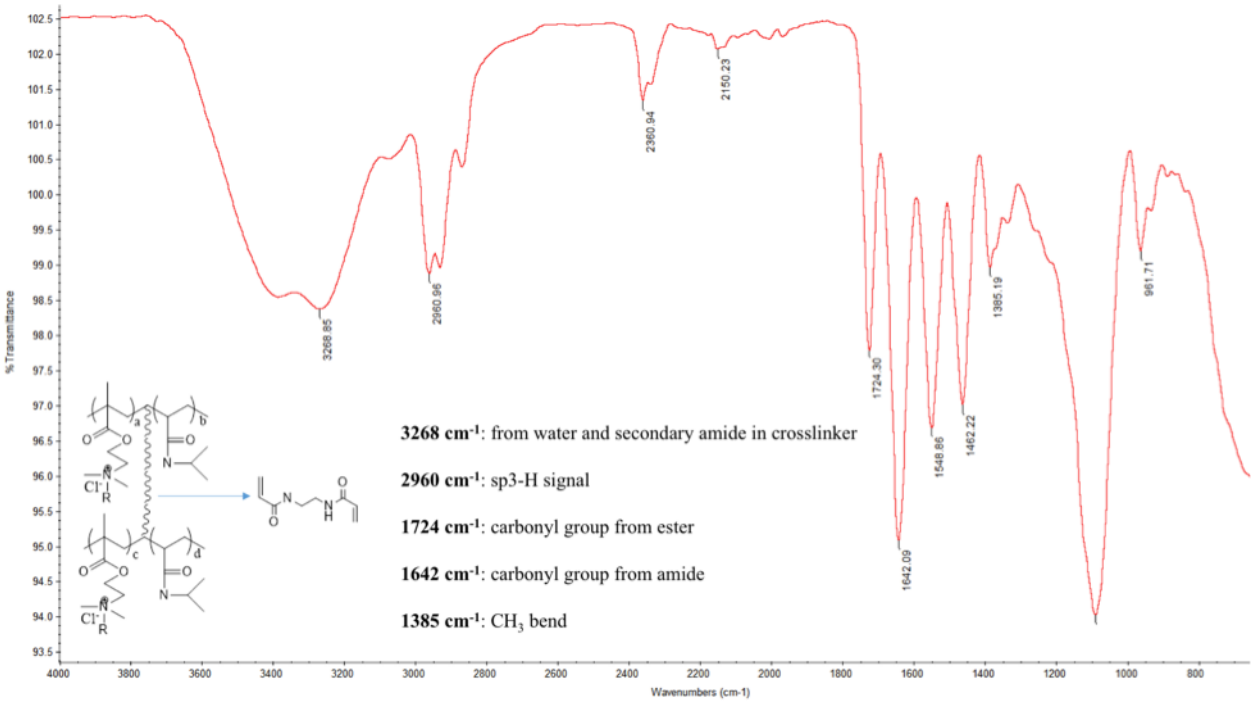

Figure 3-20 : Characterization of the polymeric hydrogel network via FT-IR

3.2.2 Preparation of Dye-Loaded Enzyme-Functionalized Hydrogel[42]

Pieces of the hydrogel were prepared (1 mm^3) to be approximately equal in dimensions. These were then soaked overnight in a mixture of the enzyme urease (2 mg/mL; 3 mL), and fluorescein dye (1 mL saturated) solution in 10 mM PBS. This enzyme/dye solution with gel particles was placed in the refrigerator overnight, and was allowed to equilibrate with room temperature before conducting experiments.

3.2.3 Monitoring Dye Release from Hydrogels Using UV-Vis Spectroscopy[42]

After allowing the hydrogels to incubate overnight in the enzyme and dye solution, they were washed 3-4 times with fresh PBS buffer to remove any adsorbed enzyme or dye molecules. Each hydrogel piece was then carefully transferred to the bottom of a UV-Vis cuvette and PBS buffer or urea solution was added to the cell. Dye release from the hydrogels was monitored with a Beckman DU-800 spectrophotometer with a 6-cell sampler, using the kinetics/time mode, with the analytical wavelength set to 488 nm, which was the maximum absorbance wavelength of fluorescein in PBS. The background wavelength used was 250 nm at 25°C. Measurements were taken every 1 hour over an 18 hour period. Dye release was monitored using 0 M, 0.005 M, 0.05 M, 0.5 M, and 1 M urea solutions in 10 mM PBS buffer. The UV-Vis absorbance values at 488 nm were then plotted as a function of time for each of these concentrations, giving the relationship between urea concentration and the quantity of dye released from the gel scaffolds.

3.2.4 Monitoring Insulin Release from Hydrogels Using UV-Spectroscopy[42]

Pieces of hydrogel were cut and incubated with enzyme as indicated above, this time using insulin as the cargo molecule. These pieces were then washed 3-4 times with Sodium Acetate Trihydrate (SAT) buffer to remove any excess enzyme and insulin molecules. The hydrogels were carefully transferred to the bottom of UV-Vis cuvettes and a solution of oxygenated SAT buffer or glucose solution was added to act as substrate and promote release of the cargo molecule. A Beckman DU-800 spectrophotometer with a 6-cell sampler was used for measurements in kinetics/time mode, with the analytical wavelength set to 276 nm, which is the maximum absorbance wavelength of insulin in SAT buffer.[27] The experiment was carried out at

25°C using 250 nm as a background wavelength. Measurements were set to be taken at periods of 60 minutes for a total time of approximately 15 hours. Initial measurements were taken 10-15 minutes after the gels were loaded into the UV-Vis cells. Insulin release from glucose oxidase-immobilized hydrogels was analyzed in 0 M, 0.05 M, 0.25 M, and 0.5 M glucose solutions. UV absorbance was plotted as a function of time for each of these concentrations, to show the direct correlation between substrate concentration and the amount of insulin molecules released from the gel.

3.2.5 Determination of Insulin Concentration Inside Hydrogel Scaffold[42]

To determine the amount of insulin released when conducting the insulin-release experiments, it was necessary to calculate the initial concentration of insulin within the hydrogel scaffold. For this calculation, experiments were performed using six gels with dimensions that were similar to those of the gels used in the release experiments. The hydrogels were soaked overnight and then washed twice with SAT buffer, as was done for the insulin release experiments. To study the gels, each of them was transferred to a UV-Vis cuvette and buffer was added to allow for passive diffusion of insulin molecules for a period of 18 hours, at 25°C. The gels in the UV-Vis cells were then triturated to ensure that the gel-absorbed insulin was released into solution. Solutions containing the gel pieces were then filtered through 0.2 μm cellulose acetate sterile syringe filters (VWR) to eliminate the compressed solid gel residues. The solutions were then transferred to new UV-Vis cuvettes and the absorbance was measured at 276 nm. The concentration of insulin in the hydrogels was then determined using the Beer-Lambert law, $A=\varepsilon bC$, where A is absorbance, ε is the molar absorptivity coefficient ($\varepsilon_{insulin}$ = 6,100 M^{-}

$^{1}cm^{-1})$[27], b is the path length (1 cm) and C is the concentration of the analyte. The average insulin concentration in solution was calculated to be 6.35 µM. The percent of insulin released from the gel in the pumping experiments were then calculated relative to this amount.

3.2.6 Synthesis and Characterization of Molecularly Imprinted Positively Charged Hydrogels

Prior to working on the synthesis of the gel itself, a petri dish and the NMR tube in which the gels were synthesized were silanized by soaking in SigmaCote (Sigma-Aldrich) for approximately 20 minutes. Methacrylic acid (MAA), Methacrylamido-propyl-trimethyl ammonium chloride (MAPTAC), and N'N methyelenebisacrylamide (BIS) were filtered through molecular sieves prior to use.

Glycerol (model molecule) (1.96 mmol) and MAA (13.57µL) were dissolved in DMSO (2 mL, Sigma-Aldrich), and the solution left for 30 minutes to allow interactions between the monomer and the model molecule take place. NIPAM (1357.92 mg), MAPTAC (39 µL), and BIS (12.33 mg) were added to the solution, and the solution was purged with nitrogen for five minutes. 2,2'-Azobis (2-methylpropionitrile) (AIBN) (3.28 mg) was then added to solution, and the solution, followed by purging with nitrogen for five minutes. The solution was then poured into a silanized test tube which continued several NMR tubes to control for diameter of the hydrogel, and then placed in a beaker upright covered with a coverglass for twenty four hours in an oven at 60°C.

Following incubation in the oven, each NMR tube was removed from the main gel matrix and the cured polymer gel was removed from the NMR tubes by cracking the glass of the NMR tubes and removing it from the outside of the gel. The gels were then dialyzed in water by

placing the finished gels in a petri dish full of water, which was replaced with fresh water every 6-8 hours. These washes were conducted over a period of two days, followed by an ethanol wash to ensure complete elimination of the model molecules and extra monomers in the hydrogel structure, plus two more days of water washes. The gels were then cut into cylindrical pieces of approximately equal size, 1 mm in height and 4 mm in diameter.

3.2.7 Monitoring 2-Pralidoxime Chloride Release from Hydrogels Using UV-Vis Spectroscopy

The gels synthesized above were then soaked in a solution of the enzyme acid or alkaline phosphatase (2mg/mL, 5 mL), PBS buffer, and a solution of 2-pralidoxime (1mg/mL, 5mL) on a mechanical shaker for 2 hours, and then placed in the refrigerator overnight. Following incubation with enzyme, the gels were washed with fresh 10 mM PBS buffer three to four times to remove any undesired molecules from the solution. Solutions of varying concentrations of sodium glycerophosphate were prepared using oxygenated 10 mM PBS buffer. The six pieces of gel were added to the UV cells, to which the various concentrations of glucose solution were added. The gels were then monitored in the UV-Vis overnight, and a graph of the data was obtained the following morning.

3.3 Results and Discussion

3.3.1 Stimuli Responsive Release of Fluorescein Dye[42]

Hydrogel scaffolds have been extensively studied since the 1980s. Many of these undergo passive or non-stimuli dependent release of substances, or generate a greater release in response to changes in the environment such as temperature, pH, or generation of electric or magnetic fields.[28-33] As a precursor to the pumps discussed in this section, studies have been previously conducted using immobilized enzymes attached to the hydrogel. These enzymes are typically affixed to the hydrogel through covalent interactions or are trapped within the polymer matrix of nanoparticles.[34-35]

The enzyme pumps demonstrated in Chapter 2 are ideal candidates for use in drug delivery. Not only is the concept of using enzymes as micropumps bio-friendly and biocompatible, the fact that it can be precisely regulated makes it a valuable resource for the generation of smart autonomous micropump devices. To demonstrate the potential of the enzyme micropumps to function as an autonomous drug delivery device, a positively charged hydrogel was created as a scaffold to immobilize enzymes and load small molecules. In the presence of substrate, fluid flows will arise in the vicinity of the gel scaffold, resulting in the active relase of cargo molecules.

A hydrogel with a quaternary ammonium functional group was synthesized and used as a new architecture for the immobilization of enzymes in the same manner as the self-assembled monolayer on the Au-patterned pumps. The hydrogel also served as a support to incorporate “guest” molecules, which for the first proof-of-concept case were fluorescein dye molecules. Given that the velocity of fluid flow increased in the Au-pattern architecture with increasing

substrate concentration, the loaded molecules should pump out of the hydrogel scaffold in a concentration-dependent manner.

To correlate absorbance values obtained in experiments involving cargo release to the concentration of the molecules being released, the creation of a calibration curve was necessary. For the study involving fluorescein dye as the cargo molecule, a calibration curve was created using various concentrations of fluorescein dye. The data points obtained for different concentrations of fluorescein in buffer were graphed in terms of absorbance vs. concentration, in order to obtain the slope of the line, which gave the absorption coefficient of the dye. The calibration curve for fluorescein dye is shown in the figure below.

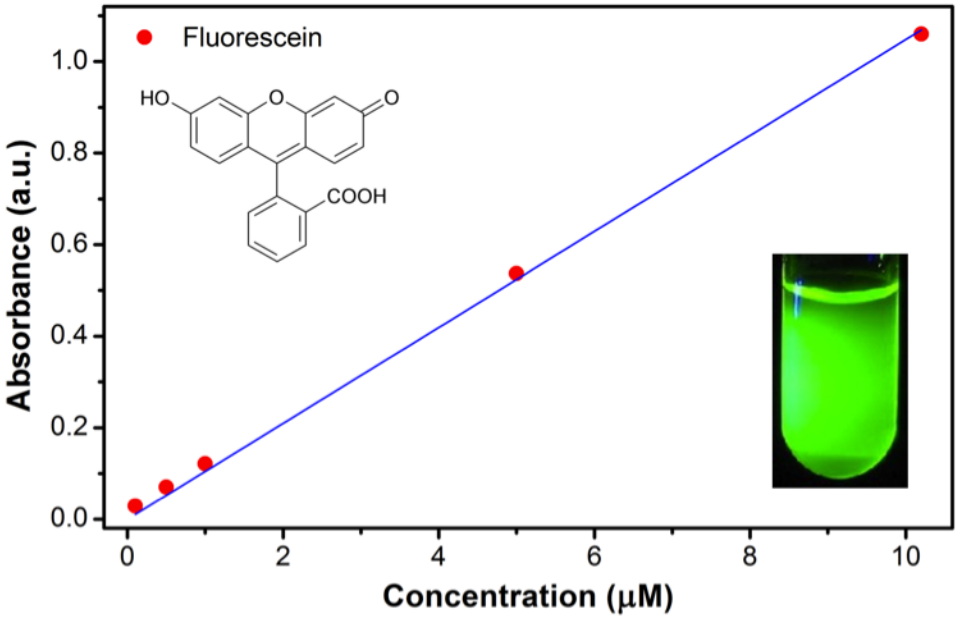

Figure 3-21 : Calibration curve for fluorescein dye in UV-Vis spectrophotometry

For the release of fluorescein molecules using the concept of enzyme pumps, the urease enzyme was attached to the hydrogel scaffold, with the fluorescein dye molecules loaded inside the gel. The synthesized cross-linked hydrogel scaffold was cut into approximately equal sized pieces, then soaked in a solution of enzyme and fluorescein dye before being washed with fresh

buffer to remove any free molecules. The release of dye was monitored in the presence of different urea solutions of variable concentrations at 488 nm. The concentrations of urea that were tested were 0.005 M, 0.05 M, 0.5 M, and 1 M urea. The results of this study are shown below in Figure 3-22.

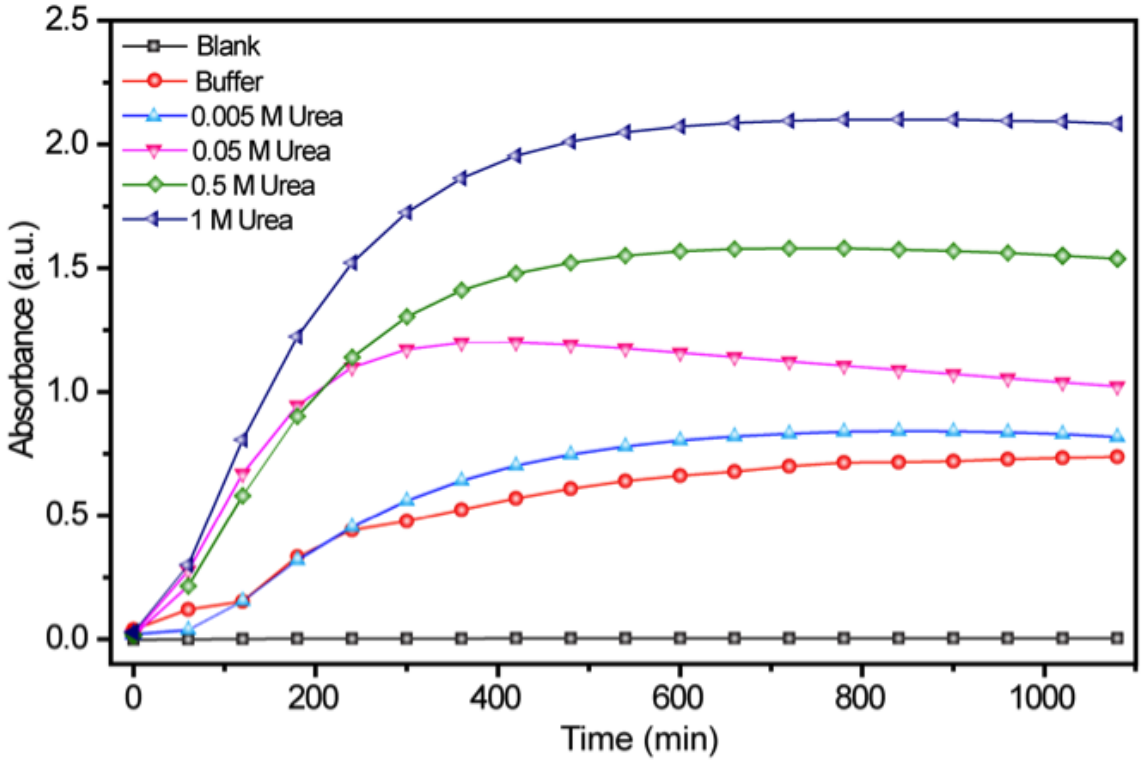

Figure 3-22 : Graph of absorbance vs. time for the release of fluorescein dye by urease in the presence of urea via UV-Vis spectrophotometry

To counteract the effects of pH on the absorbance of fluorescein dye and to provide more stability to the enzyme, the experiments were conducted in 10 mM PBS buffer. Though there was some leaching of dye molecules in the control sample with buffer, the amount of fluorescein released was clearly shown to be increasing in a concentration dependent manner given an increase in the concentration of substrate.

In order to corroborate these results, several more trials were conducted. The same trend was observed, where higher concentrations of substrate led to higher release of cargo molecules

from the gel. However, these results may have varied slightly between the trials due to the unknown quantity of dye molecules that were absorbed into the gel. Differential absorption is possible based on the characteristics of the gel in question, and there are also variations depending on the concentration of substrate available. The results from two further trials are shown graphically below.

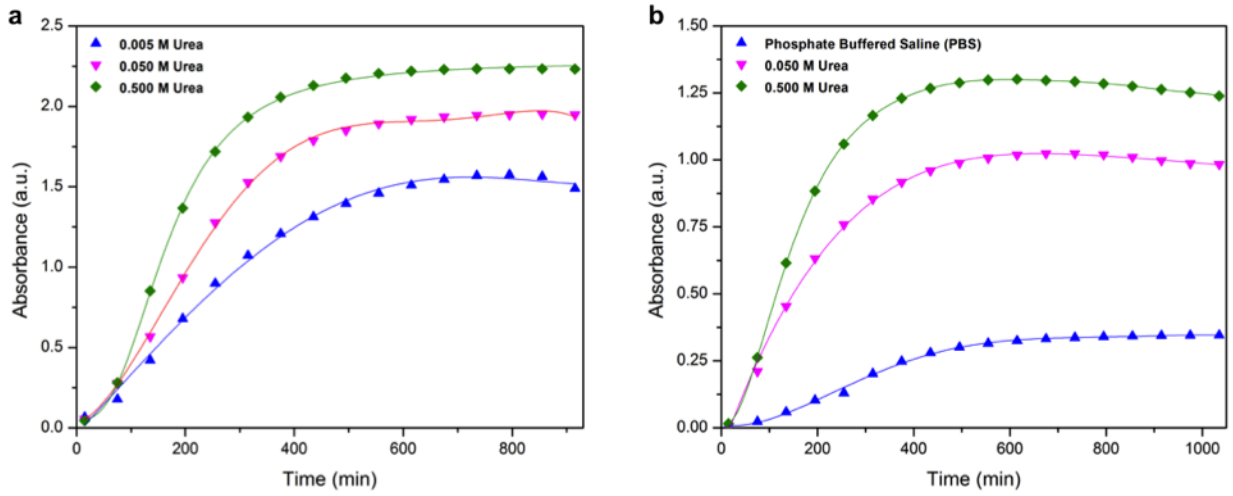

Figure 3-23 : Substrate-Mediated Release of fluorescein dye from urease-anchored hydrogels

The first trial that was conducted in (**a**) was run using 0.005 M urea, 0.050 M urea, and 0.500 M urea. As can be seen, the lowest concentration of urea had the least release of dye from the gel, while the highest concentration of urea had the most release, primarily towards the beginning of the trial. In the second trial conducted in (**b**), a control was run using just PBS buffer, and also samples were run using 0.050 M urea and 0.500 M urea.

3.3.2 Stimuli Responsive Release of Insulin[42]

Another proof-of-concept design studied included the electrostatic immobilization of glucose oxidase on hydrogel scaffolds, using insulin as a cargo molecule. For this experiment,

the pH used for the incubation of hydrogels as well as for the experiment itself was close to the isoelectric point of insulin to avoid strong binding of the molecule to the scaffold. This warranted the use of sodium acetate trihydrate (SAT) buffer, at a pH of 5.23. The buffered solution also ensured that there were no changes associated in release from the gel as a result of pH-sensitive changes in the hydrogel scaffold.

The concentrations of glucose used in these experiments were 0.005 M, 0.050 M, and 0.500 M. An oxygenated SAT buffer solution was used to make the solutions of glucose, as oxygen is a reactant necessary for the oxidation of glucose. To ensure complete saturation of the buffer with this second reactant, the buffer solution was bubbled with oxygen for one hour prior to experiments. The release profile of insulin was correlated to the total insulin absorbed into the gel, as explained in a previous section. This allowed for the calculation of the percentages of release of insulin from the gels.

For each concentration of substrate, the calculation of the concentration of insulin released was conducted using the Beer-Lambert law, where $C = \frac{A}{\varepsilon b}$. In this equation, C is concentration, A is absorbance, and ε is the molar absorptivity coefficient. For insulin, the molar absorptivity coefficient was determined from literature values to be 6,100 $M^{-1}cm^{-1}$.[27] The percentage of insulin released was determined by the concentration calculated when compared to the initial concentration of insulin in the gels, determined in the experimental section. The initial amount of insulin was found to be 6.35 μM via experimental means, thus the percentage of insulin released from the gel was calculated as:

$$\% = \frac{\left[insulin \quad released \right]}{6.35 mM} 100\%$$

As can be seen in the data tables shown in Appendix A, the percentage of insulin released from within the gel clearly increases with an increase in substrate concentration. The total percentage of insulin released throughout the entire trial of approximately 850 minutes increases from 43.9% in the SAT buffer, to 70% in the 0.500 M buffer. It should be noted that one of the concentrations tested was 0.005 M, which is an important physiological concentration of glucose and hence this proof-of-concept device is operable and effective in this concentration range. A graph of this data is shown below in Figure 3-24.

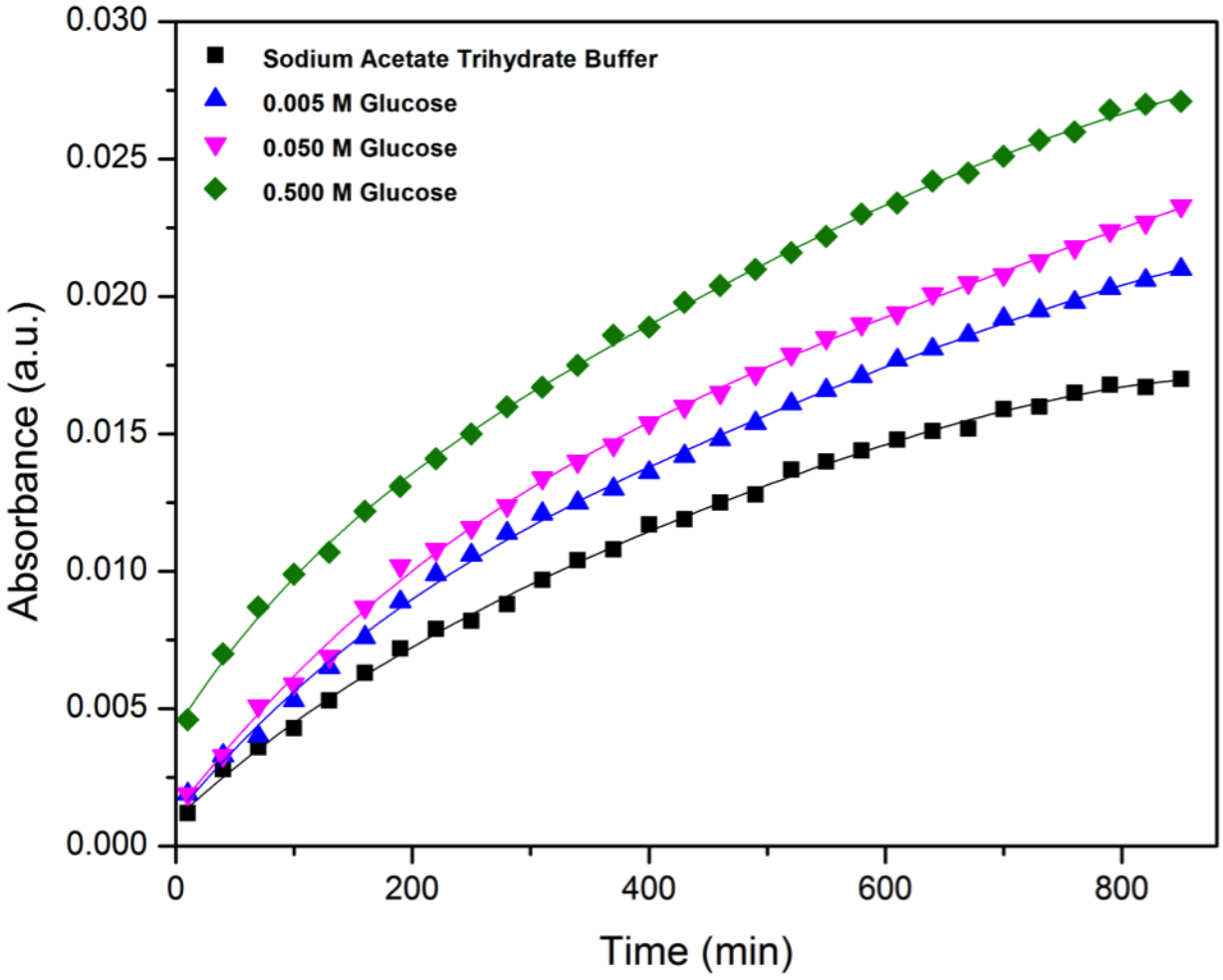

Figure 3-24 : Insulin release from glucose oxidase functionalized hydrogel scaffold in the presence of various concentrations of glucose

The black curve denotes the insulin release without substrate present, giving the background passive diffusion of insulin from within the hydrogel matrix. It was shown that the maximum release happened after approximately 800 minutes. Several trials were conducted for reproducibility, and the results of these additional experiments are displayed graphically below.

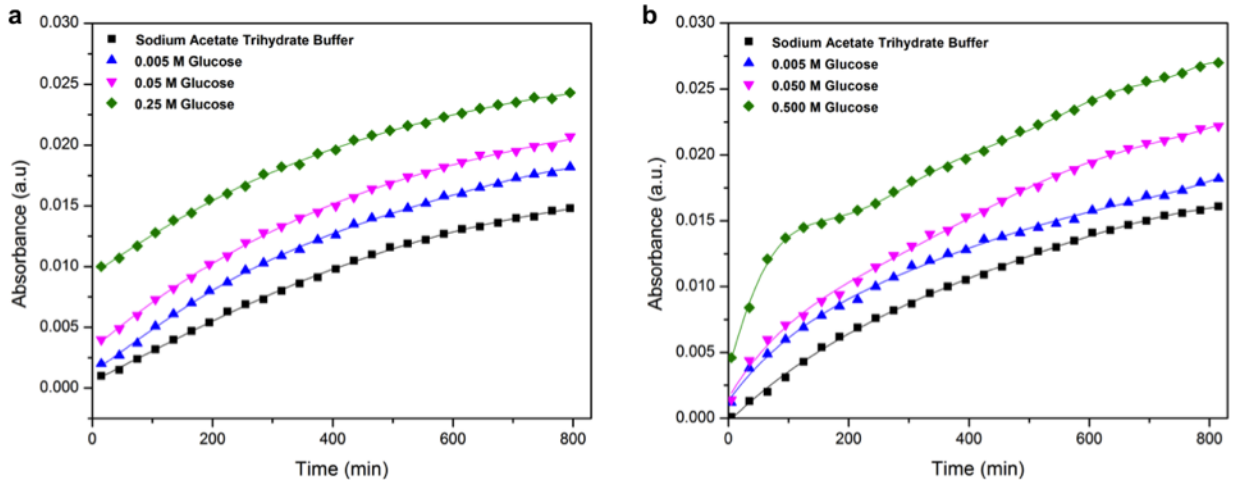

Figure 3-25 : Graphs of additional trials of glucose oxidase functionalized hydrogel scaffolds releasing insulin in response to varying concentrations of glucose

The release is shown to be fairly consistent across the various trials. For all cases, the higher the concentration of glucose, the faster the insulin is released even at the earliest time points, meaning that there is little time delay between the degradation of glucose by the enzyme and the release of insulin from the hydrogel. It can also be determined that there is a consistent difference between each concentration of substrate, and that an increase in substrate definitively causes an increase in the release of insulin both at any given time point and in an overall sense.

3.3.3 Stimuli Responsive Release of 2-Pralidoxime Chloride from Acid Phosphatase Gels

In addition to testing enzyme systems that had been previously explored, the potential applicability of this system as a sensor/pump was explored using other enzyme-substrate combinations. One of the new enzymes introduced for study in the gel scaffold was acid phosphatase. This enzyme comes from a class of lysosomal enzymes that hydrolyse organic phosphates at an acidic pH.[38] This class of enzyme is capable of hydrolyzing both a variety of biological organophosphates such as phosphoserine, adenosine triphosphate, and pyrophosphate. Additionally, they can hydrolyze selected organophosphate pesticides, such as malathion and paraoxon, which are well-known nerve agent analogues.[39-40] This gives this enzyme type significant biochemical importance in the field of nerve agent remediation and threat reduction.

As a phosphatase, this enzyme was capable of degrading a variety of different substrates. The two substrates that were tested were sodium pyrophosphate and β-glycerophosphate disodium. As we were exploring the potential for this system to be used as a treatment for nerve agent poisoning, the molecule loaded inside the gel was 2-pralidoxime (2-PAM), a potent antidote used to reverse the effects of nerve agent poisoning. These include poisons such as sarin, cyclosarin, soman, and VX, which have been investigated as possible bioweapons.[41] A schematic of the gel is shown below.

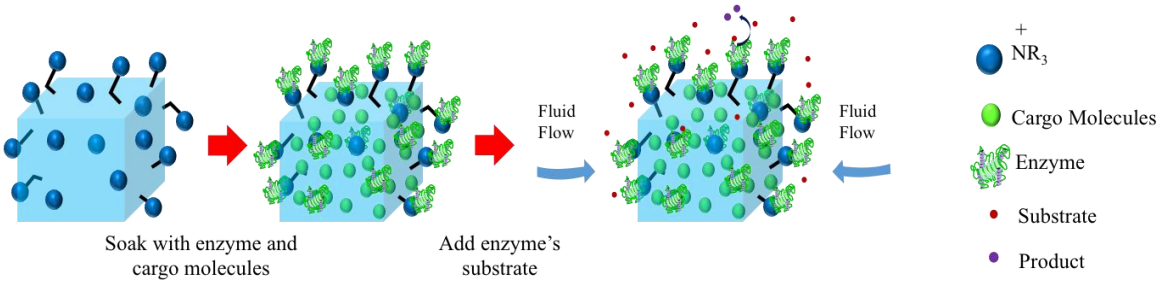

Figure 3-26 : Schema of cargo-molecule loaded enzyme-functionalized hydrogel scaffold pump

As in the previous trials with hydrogel scaffolds, the gel was synthesized such that it incorporated quaternary ammonium groups such that it could allow for electrostatic attachment of enzyme molecules on the surface. The gel was soaked with a solution of enzyme and cargo molecules, which allowed the cargo molecules to be absorbed within the gel, and the enzymes to attach to the outside. Then substrate was added, causing the enzymes to cause pumping, and hence create fluid flows that could assist in the active release of cargo molecules. The results of the trial of acid phosphatase with sodium pyrophosphate are shown graphically below in Figure 3-27.

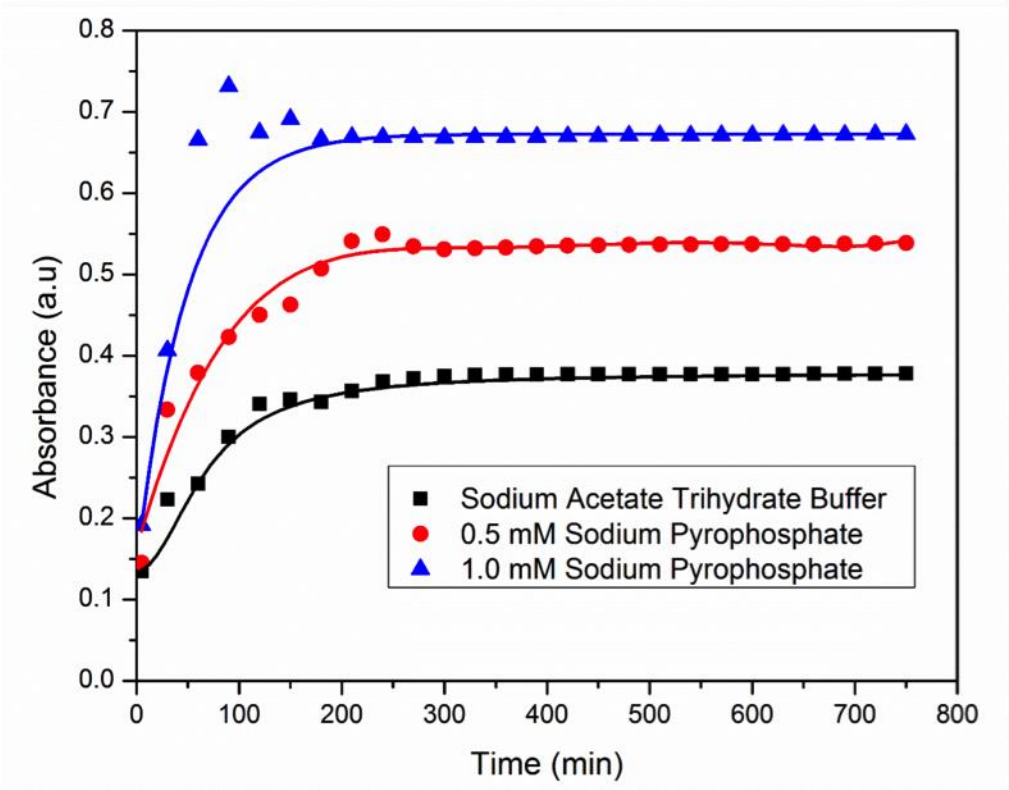

Figure 3-27 : Graph of 2-PAM loaded acid phosphatase-functionalized hydrogel scaffold with various concentrations of sodium pyrophosphate in SAT buffer

As can be seen in the graph above with the sodium pyrophosphate trials, there was an increase in the amount of cargo molecule released by the gel with an increase in substrate concentration. The trial did however have some leaching of drug molecules in the trial without

substrate molecules, indicating that there is still a contribution by passive diffusion. However, the overall concentration of drug released is significantly higher with even small quantities of substrate available.

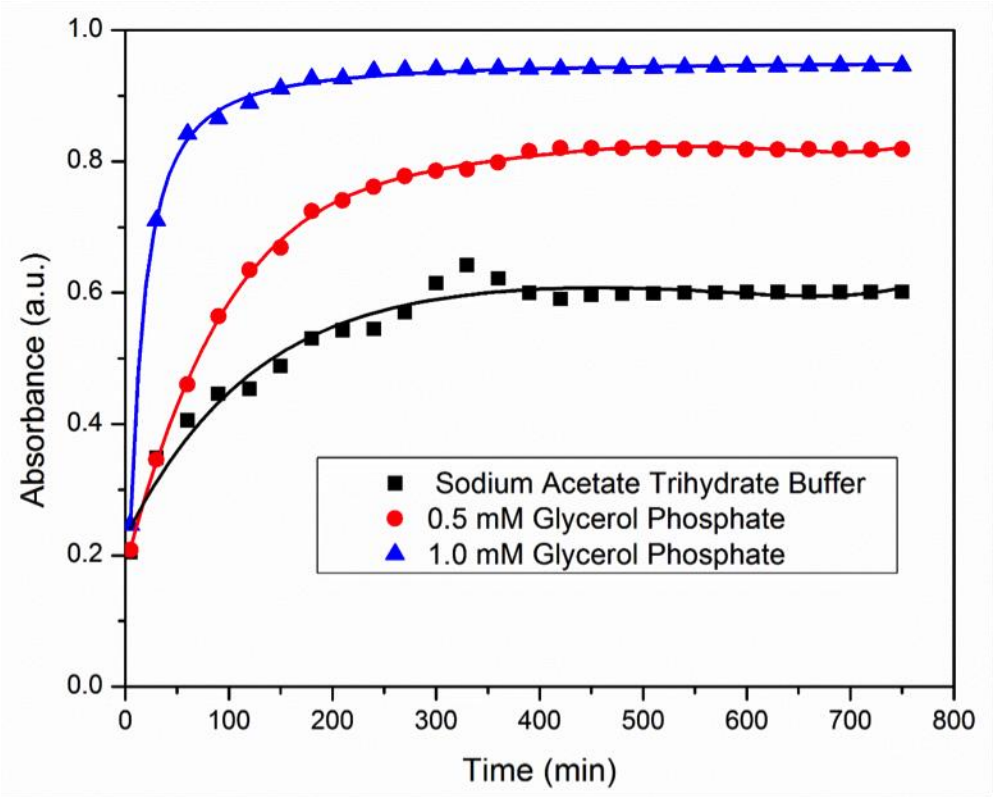

Figure 3-28 : Graph of 2-PAM loaded acid-phosphatase functionalized hydrogel scaffold with various concentrations of glycerol phosphate in SAT buffer

The release profile for the glycerol phosphate substrate was similar to that of the pyrophosphate. This implies that the release profile when considering these two substrate molecules relies heavily on the activity of the enzyme itself, rather than any other possible characteristics of the gel.

In an effort to reduce the amount of passive release of cargo molecules, the amount of passive diffusion would need to be diminished. In the previous trials with the glucose oxidase-insulin hydrogels, there was a considerable release of insulin even without the presence of

glucose, calculated to be approximately 43.9%. To help eliminate the abundance of passive diffusion, a more tightly regulated hydrogel system was used based on molecular imprinting.

Molecular imprinting has been a well-developed field for many years. This tool is typically used for separating and quantifying substances that are quite different from one another, such as drugs and bioactive molecules. Fairly recently this technology has been adapted for use in drug delivery systems, due to its ability to tightly regulate dosage and help create systems which can allow for site-specific delivery of drug molecules. Imprinted polymers have even been considered for use as drug delivery systems in plain water, using imprinted short peptides.[36]

Molecular imprinting itself creates polymer matrices with artificial recognition sites embedded within the matrix. These are generally made via co-polymerization of functional monomers and cross-linkers around a template molecule.[37] Typically, small molecules work best in molecular imprinting, and as such these copolymerization reactions cannot be well carried out in water, necessitating the use of an organic solvent for the reaction.[36] The imprinting of proteins is still typically difficult, and small pieces of proteins are often used as analogues to bind the protein of interest, without requiring the copolymerization with the whole protein. [36-37]

The definition between the absorbance values in the acid phosphatase system for even small changes in concentration of substrate made it an ideal candidate for further studies using hydrogel scaffolds. The goal of these studies was to reduce the passive diffusion of 2-PAM from the gel without any substrate present for the enzyme, by way of molecular imprinting. This type of hydrogel synthesis also facilitates the release of cargo molecules at a faster rate, as the hydrogel can be made responsive to the presence of one of the product molecules and expand, allowing for a higher release of drug molecules.

Since imprinting works best with small molecules, the hydrogel was synthesized and cross-linked in the presence of glycerol, which would serve to become the imprint. The substrate used in this case would hence be glycerophosphate disodium, which would degrade to yield glycerol, which could then adsorb into the glycerol imprints on the gel. This would help to expand the hydrogel scaffold in the presence of product, and facilitate the release of drug molecules from the gel due to the bulk solvent flow created by the pumping action of the enzymes. The data from this trial with molecularly imprinted gels is shown below in Figure 3-29.

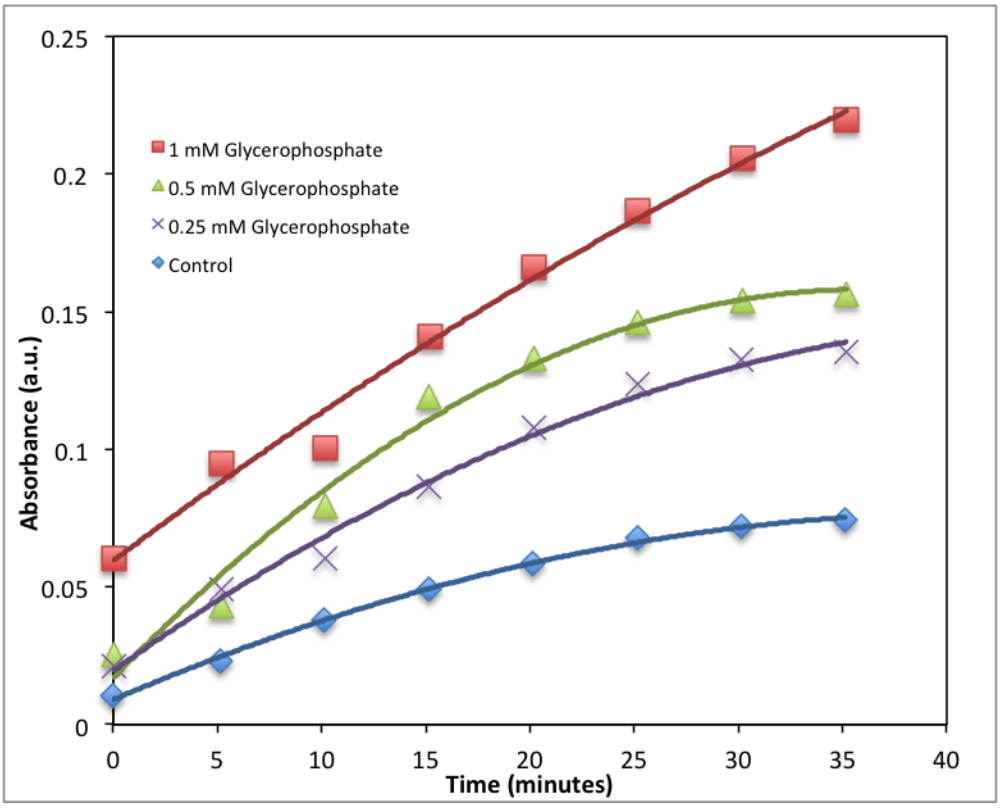

Figure 3-29 : Release of 2-PAM from molecularly imprinted hydrogel scaffold functionalized with acid phosphatase in the presence of glycerophosphate substrate

The concentrations of the glycerophosphate substrate used for this experiment were low in comparison to the previous trials. However, even at such low concentrations of substrate, there

was a marked difference between the release in the presence of substrate versus the release in buffer. It was also shown that with the molecularly imprinted hydrogels the passive release of drug molecules in the absence of substrate was decreased, and the amount of drug released from the gel was greater due to the property of the gel to respond to the presence of products when formed. This also is reflected in the time scale needed for the hydrogel to release cargo molecules, which was only approximately 40 minutes until reaching the maximal absorbance. In the previous trials, maximum release was obtained after 800 minutes. This implies that this method of hydrogel synthesis is far more efficient in terms of the release of drug molecule than previous trials, and may be better suited for applications involving antidote release, as explored with the phosphatase enzyme and 2-PAM.

3.4 Conclusion

This chapter explored the application of the previously characterized Au-pattern affixed enzyme pumps to a hydrogel scaffold system, functionalized with a loaded cargo molecule. It was demonstrated that affixing enzymes to the surface of the hydrogel could cause small molecules such as dye to be released from within the hydrogel in a concentration dependent manner. Further, it was shown that this could lead to smartly regulated autonomous devices that could release a drug molecule such as insulin in a graded manner depending on the present concentration of substrate.

It was further demonstrated that these systems could be greatly modified and improved to reduce the amount of background diffusion from the hydrogel scaffold, allowing for a more tightly regulated system. In addition, it was demonstrated that different types of enzymes could

be used to change the properties of the hydrogel release dynamics, and a molecularly imprinted hydrogel could be used in order to not only reduce passive diffusion from within the matrix, but also greatly accelerate drug delivery in the presence of very low concentrations of substrate. These findings may help fabricate smart bio-friendly sensors and pumps for the detection and sequestering of glucose from the bloodstream, or for the detection and remediation of organophosphorus toxins that may be related to bio-defense.

Chapter 4 : Conclusion

4.1 Outlook

This thesis demonstrated the fabrication and application of autonomous, ATP-independent enzyme powered micropumps. It was demonstrated that enzymes affixed to a surface could exert a force on the fluid surrounding them in the presence of their substrate in an intelligent controlled manner, and that these pumps were highly sensitive to changes in local substrate concentration. It was further demonstrated that these systems could be used for applications like drug delivery, in which case they can be immobilized on a hydrogel scaffold could cause the release of loaded drug molecules in a controlled manner, through the regulation of local substrate concentration.

The potential applications of this system are almost limitless, but there is yet much to be learned about the nature of the system. Further studies will look to incorporate a more stable attachment to surfaces, rather than the electrostatic method described in this thesis. For instance, one of the methods being explored is that of using a biotin-streptavidin-biotin assembly, which provides a strong non-covalent attachment for the fabrication of enzyme pumps. Preliminary trials have shown that this may work to increase the pumping speeds as well. Further, work will be done to determine how the system behaves in response to inhibitor concentrations. These studies will help determine the nature of pumping as the available effective concentration of enzyme decreases.

Moreover, the concept of enzyme pumps will also be applied to other enzyme-substrate combinations in order to demonstrate the applicability of these enzyme pumps as sensors in chemical warfare remediation. For this case, the response to the affixed enzyme pumps in the

presence of organophosphate molecules which cause a reversible inhibition may be investigated in the gel system, where initial pumping of an antidote could cause a reduction in the amount of enzyme inhibited. Additionally, enzymes such as phosphotriesterases could be used which would cleave the organophosphate molecules as to inactivate the warfare agent, as a possible means of treatment for an exposed individual. These could also be adapted as systems in which the gel system could be used to remediate small quantities of organophosphate agents found in water supplies.

The system will continue to be further characterized by a variety of studies in order to assess its viability and applicability to a number of systems using numerous more enzymes. This will allow the applications of the system to be increased, as well facilitate adaptations to diversity the uses of the pumps in a variety of businesses, universities, medical facilities, and industries.

APPENDIX

Time (min)	SAT Buffer		
	Absorbance (a.u.)	[Insulin] (μM)*	Percent of insulin released (%)**
10	0.0012	0.20	3.1
40	0.0028	0.46	7.2
70	0.0036	0.59	9.3
100	0.0043	0.70	1.1×10^{1}
130	0.0053	0.87	1.4×10^{1}
160	0.0063	1.0	1.6×10^{1}
190	0.0072	1.2	1.9×10^{1}
220	0.0079	1.3	2.0×10^{1}
250	0.0082	1.3	2.1×10^{1}
280	0.0088	1.4	2.3×10^{1}
310	0.0097	1.6	2.5×10^{1}
340	0.0104	1.70	26.8
370	0.0108	1.77	27.9
400	0.0117	1.92	30.2
430	0.0119	1.95	30.7
460	0.0125	2.05	32.3
490	0.0128	2.10	33.0
520	0.0137	2.25	35.4
550	0.0140	2.30	36.1
580	0.0144	2.36	37.2
610	0.0148	2.43	38.2
640	0.0151	2.48	39.0
670	0.0152	2.49	39.2
700	0.0159	2.61	41.0
730	0.0160	2.62	41.3
760	0.0165	2.70	42.6
790	0.0168	2.75	43.4
820	0.0167	2.74	43.1
850	0.0170	2.79	43.9

Table 3-5 : Absorbance values of insulin release from glucose oxidase functionalized hydrogels in SAT buffer without glucose

Time (min)	0.005 M Glucose		
	Absorbance (a.u.)	[Insulin] (μM)*	Percent of insulin released (%)**
10	0.0019	0.31	4.9
40	0.0033	0.54	8.5
70	0.0040	0.66	10
100	0.0053	0.87	14
130	0.0065	1.1	17
160	0.0076	1.3	20
190	0.0089	1.5	23
220	0.0099	1.6	26
250	0.0106	1.74	27.4
280	0.0114	1.87	29.4
310	0.0121	1.98	31.2
340	0.0125	2.05	32.3
370	0.0130	2.13	33.6
400	0.0136	2.23	35.1
430	0.0142	2.33	36.7
460	0.0148	2.43	38.2
490	0.0154	2.52	39.8
520	0.0161	2.64	41.6
550	0.0166	2.72	42.9
580	0.0171	2.80	44.1
610	0.0177	2.90	45.7
640	0.0181	2.97	46.7
670	0.0186	3.05	48.0
700	0.0192	3.15	49.6
730	0.0195	3.20	50.3
760	0.0198	3.25	51.1
790	0.0203	3.33	52.4
820	0.0206	3.38	53.2
850	0.0210	3.44	54.2

Table 3-6 : Absorbance values of insulin release from glucose oxidase functionalized hydrogels in SAT buffer with 0.005 M glucose

Time (min)	0.050 M Glucose		
	Absorbance (a.u.)	[Insulin] (μM)*	Percent of insulin released (%)**
10	0.0019	0.31	4.9
40	0.0033	0.54	8.5
70	0.0051	0.84	13
100	0.0059	0.97	15
130	0.0069	1.1	18
160	0.0087	1.4	23
190	0.0102	1.67	26.3
220	0.0108	1.77	27.9
250	0.0116	1.90	29.9
280	0.0124	2.03	32.0
310	0.0134	2.20	34.6
340	0.0140	2.30	36.1
370	0.0146	2.39	37.7
400	0.0154	2.52	39.8
430	0.0160	2.62	41.3
460	0.0165	2.70	42.6
490	0.0172	2.82	44.4
520	0.0179	2.93	46.2
550	0.0185	3.03	47.8
580	0.0190	3.11	49.1
610	0.0194	3.18	50.1
640	0.0201	3.30	51.9
670	0.0205	3.36	52.9
700	0.0208	3.41	53.7
730	0.0213	3.49	55.0
760	0.0218	3.57	56.3
790	0.0224	3.67	57.8
820	0.0227	3.72	58.6
850	0.0233	3.82	60.2

Table 3-7 : Absorbance values of insulin release from glucose oxidase functionalized hydrogels in SAT buffer with 0.050 M glucose

Time (min)	0.050 M Glucose		
	Absorbance (a.u.)	[Insulin] (μM)*	Percent of insulin released (%)**
10	0.0019	0.31	4.9
40	0.0033	0.54	8.5
70	0.0051	0.84	1.3×10^{1}
100	0.0059	0.97	1.5×10^{1}
130	0.0069	1.1	1.8×10^{1}
160	0.0087	1.4	2.3×10^{1}
190	0.0102	1.67	26.3
220	0.0108	1.77	27.9
250	0.0116	1.90	29.9
280	0.0124	2.03	32.0
310	0.0134	2.20	34.6
340	0.0140	2.30	36.1
370	0.0146	2.39	37.7
400	0.0154	2.52	39.8
430	0.0160	2.62	41.3
460	0.0165	2.70	42.6
490	0.0172	2.82	44.4
520	0.0179	2.93	46.2
550	0.0185	3.03	47.8
580	0.0190	3.11	49.1
610	0.0194	3.18	50.1
640	0.0201	3.30	51.9
670	0.0205	3.36	52.9
700	0.0208	3.41	53.7
730	0.0213	3.49	55.0
760	0.0218	3.57	56.3
790	0.0224	3.67	57.8
820	0.0227	3.72	58.6
850	0.0233	3.82	60.2

Table 3-8 : Absorbance values of insulin release from glucose oxidase functionalized hydrogels in SAT buffer with 0.500 M glucose

BIBLIOGRAPHY

1. Torchilin, V. "Recent advances with liposomes as pharmaceutical carriers" *Nat. Rev. Drug. Discov.* **2005**, 4, 145-160
2. Kataoka, K.; Harada, A.; Nagasaki, Y. "Block copolymer micelles for drug delivery: design, characterization and biological significance" *Adv. Drug Delivery Rev.* **2001**, 47, 113-131
3. Patra, D.; Sanyal, A.; Rotello, V. M. "Colloidal microcapsules: self-assembly of nanoparticles at the liquid-liquid interface" *Chem. Asian. J.* **2010**, 5, 2442-2453
4. Bassik, N.; Brafman, A.; Zarafshar, A. M.; Jamal, M.; Luvsanjay, D.; Selaru, F. M.; Gracias. D.H. "Enzymatically triggered actuation of miniaturized tools" *J. Am. Chem. Soc.* **2010**, 132, 16314-16317
5. Xi, J.; Schmidt, J. J.; Montemagno, C. D. "Self-assembled microdevices driven by muscle" *Nat. Mater.* **2005**, 4, 180-184
6. Sengupta, S., et al. Enzyme molecules as nanomotors. *J. Am. Chem. Soc.* **135**, 1406-1414 (2013).
7. Muddana, H. S., Sengupta, S. Mallouk, T. E., Sen, A. & Butler, P. J. Substrate catalysis enhances single-enzyme diffusion. *J. Am. Chem. Soc.* **132**, 2110-2111 (2010).
8. Yu, H., Jo, K., Kounovsky, K. L., de Pablo, J. J. & Schwartz, D. C. Molecular propulsion: chemical sensing and chemotaixs of DNA driven by RNA polymerase. *J. Am. Chem. Soc.* **131**, 5722-5723 (2009).

9. Voet, D., Voet, J., Pratt, C., "Enzymatic Catalysis." *Fundamentals of Biochemistry: Life at the molecular level*. 4th ed. Hoboken, NJ: Wiley, 2013. 315-367. Print.

10. Rott, N. "Note on the History of the Reynolds Number." *Annu. Rev. Fluid Mech.* **1990**. 22, 1-11

11. Purcell, E. M. "Life at Low Reynolds Number." *American Journal of Physics*. **1977**, 45, 3-11

12. Chandrasekhar, S. "Stochastic Problems in Physics and Astronomy." *Reviews of Modern Physics.* **1943**, 15:1, 20-42

13. Anderson, J. L. "Transport mechanism of biological colloids." *Annals New York Acad. Sci.* **1986**, 469, 166-177

14. Attard, P. "Electrolytes and the electric double layer." *Adv. Chem. Phys.* **1996**, 92, 1-159

15. Anderson, J. L. "Colloid transport by interfacial forces." *Annu. Rev. Fluid Mech.* **1989**, 21, 61-99

16. Wang, S.; Wu, N. "Selecting the swimming mechanisms of colloidal particles: bubble propulsion versus self-diffusiophoresis." *Langmuir*. **2014**, 30 (12), 3477-3486

17. Gaetani, G.; Ferarris, A.; Rolfo, M.; Mangerini, R.; Arena, S.; Kirkman, H. "Predominant role of catalase in the disposal of hydrogen peroxide within human erythrocytes." *Blood*. **1996**, 87, 1595-1599

18. Axellson, I.; "Characterization of proteins and other macromolecules by agarose gel chromatography." *J. Chrom.* **1978**, 152, 21-32

19. Switala, J.; Loewen, P.C. "Diversity of properties among catalases." *Arch. Biochem. Biophys.* **2002**, 27, 145-154

20. Svendsen, A. "Lipase protein engineering." *Biochim. Biophys. Acta.* **2000**, 1543, 223-228

21. Qian, Z.; Lutz, S. “Improving the catalytic activity of Candida Antarctica lipase B by circular permutation.” *J. Am. Chem. Soc.* **2005**, 127 (39), 13466-13467

22. Raba, J; Mottola, H. A. “Glucose oxidase as an analytical reagent.” *Critical Rev. Anal. Chem.* **1995**, 25, 1-42

23. Kalisz, H. M.; Hecht, H. J.; Schomburg, D.; Schmid, R. D. “Effects of carbohydrate depletion on the structure, stability, and activity of glucose oxidase from Aspergillus niger.” *Biochim. Biophys. Acta. Protein Struct. Mol. Enzymol.* **1991**, 1080 (2), 138-142

24. Hyon, S. H.; Cha, W.I.; Ikada, Y. “Preparation of transparent poly(vinyl alcohol) hydrogel.” *Polymer Bulletin*. **1989**, 22, 119-122

25. Kopecek, J. “Hydrogel biomaterials: A smart future?” *Biomaterials*. **2007**, 28, 5185-5192

26. Ravikumar, T; Murata, H.; Koepsel, R. R.; Russell, A. J.; “Surface-active antifungal polyquaternary amine.” *Biomacromolecules* **2006**, 7, 2762-2769

27. Gammeltoft, S. “Receptor binding of biosynthetic human insulin on isolated pig hepatocytes.” *Diabetes Care.* **1981**, 4 (2), 235-237

28. Hoffman, A. S. “ “Intelligent” polymers in medicine and biotechnology” *Macromol. Symp.* **1995**, 98, 645-664

29. Hsieh, D. S. T.; Langer, R.; Folkman, J. “Magnetic modulation of release of macromolecules from polymers” *Proc. Natl. Acad. Sci. USA* **1981**, 78, 1863-1867

30. Peppas, N. A.; Hilt, J. Z.; Kademhosseini, A.; Langer, R. “Hydrogels in biology and medicine: from molecular principles to bionanotechnology” *Adv. Mater*. **2006**, 18, 1345-1360

31. Miyata, T.; Asami, N.; Uragami, T. "A reversibly antigen-responsive hydrogel" *Nature* **1999**, 399, 766-769

32. Wood, K. C.; Zacharia, N. S.; Schmidt, D. J.; Wrightman, S. N.; Andaya, B. J.; Hammond, P. T. "Electroactive controlled release thin films" *Proc. Natl. Acad. Sci. USA* **2008**, 105, 2280-2285

33. Zhao, X.; Kim, J.; Cezar, C. A.; Huebsch, N.; Lee, K.; Bouhadir, K.; Mooney, D. J. "Active scaffolds for on-demand drug and cell delivery" *Proc. Natl. Acad. Sci. USA* **2010**, 108, 67-72

34. Galaev, I. Y.; Mattiasson, B. " 'Smart' polymers and what they could do in biotechnology and medicine" *Trends Biotechnol.* **1999,** 17, 335-340

35. Gu, Z.; Aimetti, A. A.; Wang, Q.; Dang, T. T.; Zhang, Y.; Veiseh, O.; Cheng, H.; Langer, R. S.; Anderson, D. G. "Injectable nano-network for glucose mediated insulin delivery" *ACS Nano.* **2013**, 7 (5), 4194-4201

36. Alvarez-Lorenzo, C.; Concheiro, A. "Molecularly imprinted polymers for drug delivery." *Journal of Chromatography B.* **2004**, 804, 231-245

37. Bossi, A.; Bonini, F.; Turner, A. P. F.; Piletsky, S. A. "Molecularly imprinted polymers for the recognition of proteins: The state of the art." *Biosensors and Bioelect.* **2007**, 22, 1131-1137

38. Henneberry, M. O.; Engel, G.; Grayhack, J. T. "Acid phosphatase." *Urol Clin. North Am.* **1979**, 6 (3), 629-41

39. Hoehamer, C. F.; Mazur, C. S.; Wolfe, N. L. "Purification and partial characterization of an acid phosphatase from Spirodela oligorrhiza and its affinity for selected organophosphate pesticides" *J. Agric. Food. Chem.* **2005**, 53 (1), 90-97

40. LeJeune, K. E.; Russell, A. J. “Covalent binding of anerve agent hydrolyzing enzyme with polyurethane foams” *Biotechn. And Bioeng.* **2000**, 51 (4), 450-457

41. Stojiljkovic, M.; Jokanovic, M. “Pyridinium oximes: rationale for their selection as causal antidotes against organophosphate poisonings and current solutions for auto-injectors” *Arh Hig Rada Toksikol*. **2006**, 57, 435-443

42. Sengupta, S.; Patra, D.; Rivera, I. O.; Agrawal, A.; Shklyaev, S.; Dey, K. K.; Figueroa, U. C.; Mallouk, T. E.; Sen, A. “Self-powered enzyme micropumps” *Nature Chem.* **2014**, 6, 415-422

43. Miranda, O. R.; Chen, H. T.; You, C. C.; Mortenson, D. E.; Yang, X. C.; Bunz, U. H. F.; Rotello, V. M. “Enzyme-amplified array sensing of proteins in solution and in biofluids.” *J. Am. Chem. Soc.* **2010**, 132 (14), 5285-5289

Arjun Agrawal
344 Abrams Mill Road
King of Prussia, PA 19406

Arjun@octalk.com
(484) 919-6077

ARJUN AGRAWAL

Academic Vitae

EDUCATION:

Milton S. Hershey College of Medicine, The Pennsylvania State University *Hershey, PA*
Doctor of Medicine, Anticipated May 2019

Schreyer Honors College, The Pennsylvania State University *University Park, PA*
Bachelors of Science in Biology-Neuroscience, May 2015
Honors in Chemistry

Montgomery County EMS Training Institute, School of Public Safety *Norristown, PA*
Pennsylvania Certified Emergency Medical Technician, August 2011

University of Pennsylvania, School of Arts and Sciences *Philadelphia, PA*
Pre-College Program, Non-degree Coursework, 2009-2010

Upper Merion Area High School, Upper Merion Area School District *King of Prussia, PA*
Graduated **Valedictorian**, June 2011

RESEARCH EXPERIENCE:

Undergraduate Researcher, Sen Nanomotor Group, Dept. of Chemistry *University Park, PA*
Summer 2012-Spring 2015
Worked on Novel Enzymatic nanomotor micropumps, hydrogel scaffolds with enzyme pump functionality, and enzyme microcapsules as pumps

PUBLICATIONS:

Nature Chemistry; "Self-powered enzyme micropumps" **2014**, 6, 415-422
Sengupta, S.; Debabrata, P.; Rivera, I. O.; Agrawal, A.; Shklyaev, S.; Dey, K. K.; Figueroa, U. C.; Mallouk, T. E.; Sen, A.

CLINICAL EXPERIENCE:

Emergency Medical Technician, Community Ambulance Association of Ambler *Ambler, PA*
June 2011-October 2014; Volunteer EMT-B

Observational Intern, Dr. Sanjay Gupta, MD, Trauma & Emergency Surgeon *Nashua, NH*
at Southern New Hampshire Medical Center and Intensivist/Trauma Surgeon at *Boston, MA*
Massachusetts General Hospital
May, 2013; Observed a variety of surgeries and procedures and rounded with physicians

Shadow Experience, Dr. Vijaypal Arya, MD, Gastroenterologist at Wyckoff Heights Hospital and private practice — Brooklyn, NY

Summer 2012; Observed a variety of procedures and spoke with patients and their families

WORK EXPERIENCE:

Executive Assistant and Marketing Director, Object CTalk Inc. — *King of Prussia, PA*

2007-Present; Engaged in upkeep tasks of the business and designed and implemented various marketing platforms

VOLUNTEER EXPERIENCE:

Independent Activist, Ekal Vidyalaya – One Teacher School Initiative

Raised funds and awareness for non-profit organization to establish schools in remote villages in India

Independent Fundraiser, Sankara Eye Foundation

Raised funds for non-profit organization that provides free eye surgeries for poor people in India

HONORS AND AWARDS:

Schreyer Honors College Scholar, The Pennsylvania State University
Dean's List; Semesters 1-8 at The Pennsylvania State University
Member of the Golden Key International Honour Society
Member of the National Society of Collegiate Scholars
Member of Alpha Epsilon Delta, The Premedical Honor Society
General Chemistry Laboratory A+ Award, The Pennsylvania State University
Graduated Valedictorian from Upper Merion Area High School
Featured in 6ABC's Best of the Class 2011
Featured as a full-page article in The Times Herald of Norristown